Electronic Structures and Spin Topologies of γ-Picoliniumyl Radicals. A Study of the Homolysis of *N*-Methyl-γ-picolinium and of Benzo-, Dibenzo-, and Naphthoannulated Analogs

Rainer Glaser,*,† Yongqiang Sui,† Ujjal Sarkar,† and Kent S. Gates*,†,‡

Departments of Chemistry and Biochemistry, University of Missouri-Columbia, Columbia, Missouri 65211

Received: February 9, 2008

Radicals resulting from one-electron reduction of (*N*-methylpyridinium-4-yl) methyl esters have been reported to yield (*N*-methylpyridinium-4-yl) methyl radical, or *N*-methyl-γ-picoliniumyl for short, by heterolytic cleavage of carboxylate. This new reaction could provide the foundation for a new structural class of bioreductively activated, hypoxia-selective antitumor agents. *N*-methyl-γ-picoliniumyl radicals are likely to damage DNA by way of H-abstraction and it is of paramount significance to assess their H-abstraction capabilities. In this context, the benzylic C−H homolyses were studied of toluene (**T**), γ-picoline (**P**, 4-methylpyridine), and *N*-methyl-γ-picolinium (**1c**, 1,4-dimethylpyridinium). With a view to providing capacity for DNA intercalation the properties also were examined of the annulated derivatives **2c** (1,4-dimethylquinolinium), **3c** (9,10-dimethylacridinium), and **4c** (1,4-dimethylbenzo[*g*]quinolinium). The benzylic C−H homolyses were studied with density functional theory (DFT), perturbation theory (up to MP4SDTQ), and configuration interaction methods (QCISD(T), CCSD(T)). Although there are many similarities between the results obtained here with DFT and CI theory, a number of significant differences occur and these are shown to be caused by methodological differences in the spin density distributions of the radicals. The quality of the wave functions is established by demonstration of internal consistencies and with reference to a number of observable quantities. The analysis of spin polarization emphasizes the need for a clear distinction between "electron delocalization" and "spin delocalization" in annulated radicals. Aside from their relevance for the rational design of new antitumor drugs, the conceptional insights presented here also will inform the understanding of ferromagnetic materials, of spin-based signaling processes, and of spin topologies in metalloenzymes.

Introduction

The redox reactions of quaternized nitrogen heterocycles, including both heterocyclic *N*-oxides and *N*-alkylated heterocycles, are chemically and biologically interesting. For example, the herbicide methyl viologen (paraquat) and the promising antitumor agent tirapazamine (Scheme 1) possess potent cytotoxic properties that stem from their propensity to undergo enzymatic one-electron reduction inside cells.[1–6] Understanding the fate of the organic radicals resulting from one-electron reduction of these compounds is crucial for understanding their biological properties. In the case of paraquat, the radical reacts readily with molecular oxygen to regenerate paraquat and one equivalent of superoxide $O_2^{\bullet-}$.[1–4] The repeated enzymatic reduction and back-oxidation by O_2, i.e., the redox-cycling, can generate significant amounts of intracellular superoxide. Although cells contain enzyme systems that destroy $O_2^{\bullet-}$ and its decomposition product H_2O_2, redox-cycling can overwhelm these protective mechanisms with deleterious results to the cell.[7] Similarly, tirapazamine undergoes redox-cycling under aerobic conditions.[5,6,8–11] Under low-oxygen (hypoxic) conditions, however, alternative reaction channels become available and the tirapazamine-derived radical can decompose either by homolytic N−O fragmentation and hydroxyl radical release or by way of dehydration to yield a benzotriazinyl radical.[12,13] Regardless of the exact mechanism, it is clear that tirapazamine radical anion reacts to yield a potent DNA-damaging species under hypoxic conditions.[13–17] The reactive intermediate generated under low-oxygen conditions is significantly more cytotoxic than the superoxide radical generated under aerobic conditions and, as a result, tirapazamine displays selective toxicity against the hypoxic cells found in solid tumors.[6] Accordingly, the efficacy of tirapazamine as an anticancer drug is currently being tested in a variety of phase I, II, and III clinical trials.[18]

Radicals resulting from one-electron reduction of (*N*-methylpyridinium-4-yl) methyl esters have been reported to undergo heterolysis to yield a carboxylate and (*N*-methylpyridinium-4-yl) methyl radical (Scheme 1, right).[19,20] This process has been examined as part of a program aimed at developing photolabile carboxylate protecting groups. This interesting reaction could also provide the foundation for a new structural class of bioreductively activated, hypoxia-selective antitumor agents, in which a potential DNA-damaging radical is released selectively following one-electron reduction of the parent (*N*-methylpyridinium-4-yl) methyl ester under the low-oxygen conditions found inside solid tumors. Although the DNA-damaging properties of carbon-centered alkyl radicals are well-known,[21–23] the reactions of (*N*-methylpyridinium-4-yl) alkyl radicals with nucleic acids have not yet been examined and, in fact, this particular type of radical been has been discussed as reactive intermediates only in a few cases.[24] The (*N*-methylpyridinium-4-yl) alkyl radicals are likely to damage DNA by way of H-abstraction and it is an open question as to whether this event

* Corresponding authors. E-mail: R.G., glaserr@missouri.edu; K.S.G., gatesk@missouri.edu.
† Department of Chemistry.
‡ Department of Biochemistry.

10.1021/jp8011987 CCC: $40.75
Published on Web 05/22/2008

SCHEME 1: Radicals Formed under Hypoxic Conditions

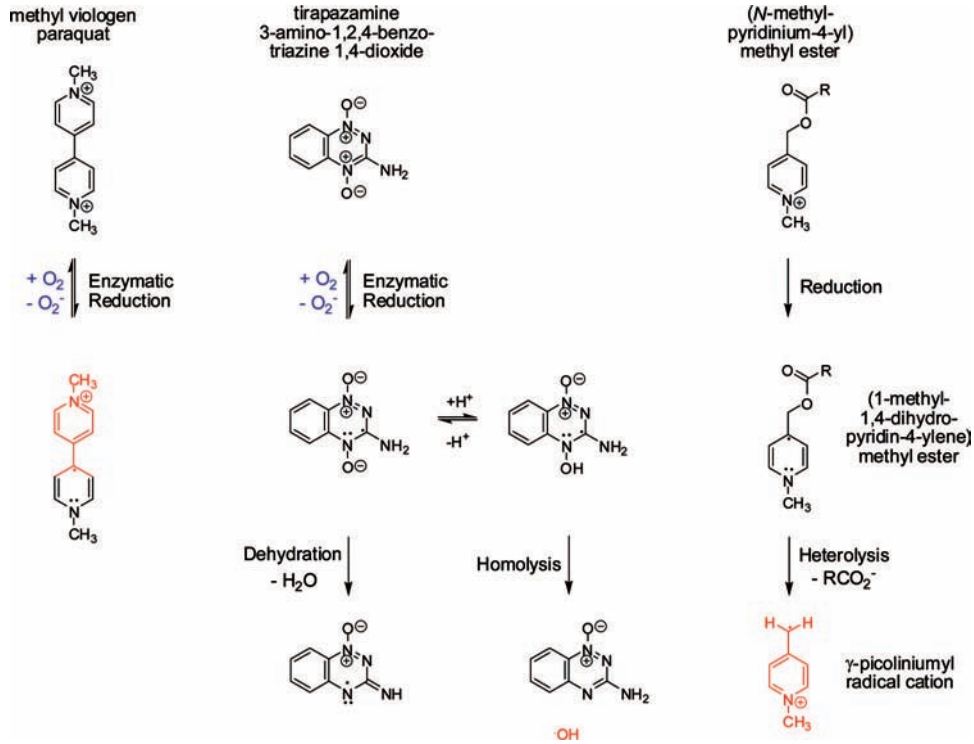

SCHEME 2: Homolyses of Toluene (T → TR + H), γ-Picoline (P → PR + H), *N*-Methyl-γ-picolinium (1c → 1rc + H), and Annulated 1c-Derivatives 2c−4c

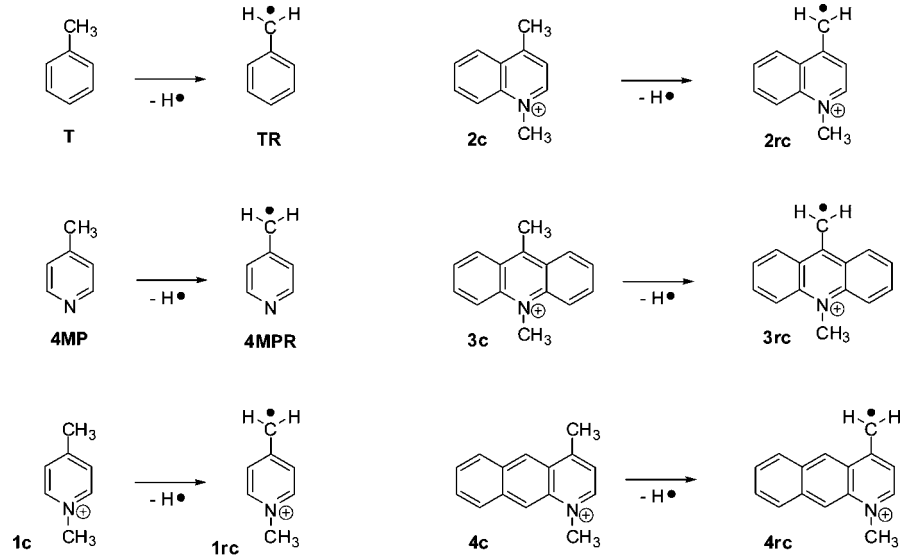

would result from direct reaction or would involve the prior reaction with O_2 to generate the corresponding peroxy radicals.

In this article, we report on the benzylic C−H homolyses of toluene (**T**), γ-picoline (**4MP**, 4-methylpyridine, or **P** for short), and *N*-methyl-γ-picolinium (**1c**, 1,4-dimethylpyridinium), and of the benzo-, dibenzo- and naphthoannulated **1c**-derivatives **2c** (1,4-dimethylquinolinium), **3c** (9,10-dimethylacridinium), and **4c** (1,4-dimethylbenzo[*g*]quinolinium). The benzylic C−H homolyses $R-CH_3 \rightarrow R-CH_2^{\bullet} + H^{\bullet}$ (Scheme 2) were studied with density functional theory (DFT), Møller−Plesset perturbation theory (up to MP4SDTQ), and higher-level configuration interaction theory (QCISD(T), CCSD(T)). These radical stabilities are of paramount significance to assess the H-abstraction capabilities of **1rc**−**4rc**. Although the properties of C−H bonds of the methyl groups should not be altered drastically by remote CH/N or CH/NCH_3^+ replacement, the assessment of the effects of this replacement on the electronic structures of the benzyl radicals $R-CH_2^{\bullet}$ is nontrivial. With a view to applications in medicinal chemistry we also examined properties of annulated derivatives. Compounds of this type are expected to possess capacity for intercalation and annulation presents one strategy to increase DNA binding.[25] In addition to understanding the effects of annulation on the stabilities of the annulated radicals, it is equally important to investigate whether and in what ways the remote CH/N or CH/NCH_3^+ replacements affects the electron and spin distributions. Molecular electrostatic potentials, electron and spin density distributions, and fragment populations have been determined to inform these issues.

Though there are many similarities between the results obtained here with DFT and CI theory, significantly different

TABLE 1: Bond Dissociation Energies[a]

parameter	theor level	T	P	1	2	3	4
BDE	B3LYP	94.90	95.99	95.26	94.83	92.13	94.17
	MP2	112.13	115.12	107.45	125.66	100.00	101.78
	PMP2,*s*+1	89.19	91.96	92.23	93.39	94.03	91.34
	PMP2,*s*+4	94.22	96.96	94.42	103.79	94.11	92.55
	PMP3,*s*+4	89.52	91.28	91.28	95.23	94.11	91.25
	PMP4,*s*+4	92.25	94.57	94.05	100.17	94.00	93.48
	QCISD[b]	92.16	93.85	93.47	97.40	93.98	93.51
	QCISD(T)[b]	93.38	95.09	94.46	98.69		
	CCSD[b]	91.90	93.46	93.20	96.39		
	CCSD(T)[b]	93.47	95.17	95.07	98.75		
BDH_0	B3LYP	86.48	87.57	87.16	86.54	83.89	85.79
	PMP4,*s*+4	85.10	87.41	87.75	94.86	89.14	88.46
	QCISD[b]	85.01	86.69	87.18	92.09	89.12	88.49
	QCISD(T)[b]	86.23	87.93	88.16	93.37		
	CCSD[b]	84.75	86.31	86.90	91.08		
	CCSD(T)[b]	86.32	88.01	88.77	93.43		
BDH_{298}	B3LYP	87.07	88.15	87.67	87.22	84.42	86.49
	PMP4,*s*+4	85.52	87.86	88.15	96.07	89.91	89.40
	QCISD[b]	85.43	87.14	87.57	93.30	89.89	89.43
	QCISD(T)[b]	86.65	88.38	88.56	94.59		
	CCSD[b]	85.17	86.75	87.29	92.29		
	CCSD(T)[b]	86.74	88.46	89.17	94.65		
BDG	B3LYP	79.57	80.66	80.75	79.07	77.06	78.24
	PMP4,*s*+4	78.21	80.53	81.06	88.77	82.94	81.54
	QCISD[b]	78.12	79.81	80.49	86.00	82.91	81.57
	QCISD(T)[b]	79.35	81.05	81.48	87.29		
	CCSD[b]	77.86	79.42	80.21	84.99		
	CCSD(T)[b]	79.44	81.13	82.08	87.34		

[a] All data in kcal/mol. [b] Using MP2 thermochemical data; see text.

results occur for some cases and these differences are shown to reflect methodological differences in the spin density distributions of the radicals. Although spin polarization enters naturally in valence bond thought culture,[26] the computational methods most widely employed by chemists are based on LCAO-MO theory and the concept of spin polarization has not been well developed outside of the small circle of theorists. Because we argue for the correctness of nonintuitive results, it was thought imperative to establish the quality of the wave functions inasmuch detail as possible and internal consistencies are demonstrated with reference to a number of observable quantities. The discussion of spin polarization emphasizes the need for a clear distinction between "electron delocalization" and "spin delocalization". The neglect of this distinction in many cases remains without consequence in qualitative analysis, but to ignore the distinction can lead to unwarranted presumptions and missed opportunities about long-range magnetic effects in organic radicals. The analysis produces conceptional insights that allow for judgments regarding the accuracy of the results of the present theoretical study and their meaning for experimentalists. Aside from the medicinal chemistry perspective, the concepts also might inform the understanding of the electronic structure of ferromagnetic materials,[27,28] of spin-based signal processing devices,[29] and of spin topologies in metalloenzymes.[30]

Theoretical and Computational Methods. Restricted Hartree−Fock theory (RHF) presents a good starting point for theoretical studies of closed-shell molecules, whereas studies of radicals with restricted open-shell or unrestricted Hartree−Fock theories (ROHF and UHF),[31] present their own special advantages and challenges.[32] In ROHF theory the unpaired electron(s) are not allowed to interact with the paired electrons individually and spin polarization is thus neglected. In contrast, every electron is described by its own spin−orbital in UHF theory and an unpaired electron affects α- and β-electrons differently. However, this approach suffers from spin contamination, that is, an overestimation of spin polarization due to the admixture of higher spin states $s + n$ ($n = 1, 2, ..., m$). The post-HF application of projection techniques[33,34] allows for the annihilation of spin states $s + n$ and the determination of PUHF(s+m) energies. The contribution of the next higher spin state often dominates the total spin contamination; the largest improvement is associated with the step from UHF to PUHF(s+1) and the spin contamination is completely removed at the PUHF(s+4) level.

Spin polarization intrinsically is a correlation effect, correlated methods are required to compute meaningful spin densities, and the spin densities become more accurate the more correlation is covered. In practice, this is often accomplished with *x*th-order Møller−Plesset perturbation theory (MPx, i.e., up to MP4-SDTQ)[35,36] and perturbation theory including spin projection (PMPx(s+n)).[37] Configuration interaction theory[38] is a more rigorous alternative, and we employed quadratic configuration interaction (QCI) and coupled cluster (CC) theory. All single and double excitations were included in the configuration space (QCISD, CCSD) and triple excitations were included subsequently as perturbations (QCISD(T), CCSD(T)). The UHF-CCSD method eliminates the (s+1) spin contaminant completely and largely removes most of the higher spin contaminants.[37,39]

Studies of radicals have become more frequent with the maturation of DFT methods, and especially the hybrid method B3LYP has become widely used and accepted.[40] Spin contaminations of unrestricted Kohn−Sham wave functions often are moderate, and this has been the implicit justification for the application of DFT in studies of radicals even though problems with spin-projected DFT occur[41,42] and general conceptual limitations exist.[43]

The structures of the closed-shell molecules **T**, **P**, and **1c**−**4c** were optimized at the theoretical levels RB3LYP/6-31G* and RMP2/6-31G* and those of the radicals **TR**, **PR** (short for

TABLE 2: Electron Density Distribution in Toluene (T), γ-Picoline (P), and *N*-Methyl-γ-picolinium Ions 1c−4c

	B3LYP						QCI					
atom or fragment	**T**	**P**	**1c**	**2c**	**3c**	**4c**	**T**	**P**	**1c**	**2c**	**3c**	**4c**
CH_3	0.03	0.04	0.11	0.10	0.09	0.10	0.03	0.04	0.11	0.10	0.09	0.09
$C(CH_3)$	−0.03	0.00	0.08	0.11	0.15	0.12	−0.04	0.00	0.08	0.12	0.17	0.13
$C-CH_3$	0.00	0.04	0.19	0.21	0.25	0.22	0.00	0.04	0.19	0.22	0.26	0.23
C_o-H in **1**, **2** and **4**	0.00	−0.04	0.05	0.01		−0.01	0.00	−0.04	0.04	−0.01		−0.03
C_m-H in **1**, **2** and **4**	0.01	0.25	0.35	0.38		0.38	0.01	0.25	0.35	0.39		0.40
C_o in C_2H_2	−0.23	−0.27	−0.23	−0.27		−0.29	−0.23	−0.27	−0.24	−0.28		−0.30
C_m in C_2H_2	−0.23	0.02	0.08	0.11		0.12	−0.22	0.03	0.08	0.13		0.14
C_o in C_2R_2				−0.08	−0.10	−0.09				−0.08	−0.11	−0.10
C_m in C_2R_2				0.21	0.24	0.18				0.20	0.25	0.18
C_2H_2 in **1**, **2** and **4**	0.01	0.21	0.39	0.38		0.37	0.01	0.20	0.39	0.38		0.37
$C_2C_4H_4$ in **2** and **3**				0.39	0.39					0.37	0.37	
$C_2C_8H_6$ in **4**						0.41						0.38
hydrocarbon	0.01	0.42	0.79	0.77	0.77	0.78	0.01	0.41	0.78	0.76	0.74	0.76
Δ(CH) in C_2H_2	0.01	0.28	0.30	0.37		0.40	0.01	0.29	0.31	0.40		0.43
Δ(C) in C_2H_2	0.00	0.30	0.31	0.38		0.41	0.01	0.30	0.32	0.41		0.45
Δ(C) in C_2R_2				0.28	0.33	0.28				0.29	0.36	0.28
N, C_p in **T**	−0.24	−0.46	−0.31	−0.30	−0.31	−0.30	−0.24	−0.45	−0.30	−0.29	−0.31	−0.29
$H_3C(N)$, $H(C_p)$ in **T**	0.23		0.33	0.31	0.29	0.31	0.23		0.33	0.32	0.30	0.31
H_3C-N, HC_p in **T**	−0.01		0.02	0.01	−0.02	0.00	−0.01		0.03	0.03	0.00	0.02
Me-C and N-Me			0.21	0.23	0.23	0.22			0.22	0.24	0.26	0.24

TABLE 3: Electron Density Distributions of Benzyl Radical TR, γ-Picolinyl Radical PR, and *N*-Methyl-γ-picoliniumyl Radical Cations 1rc−4rc

	B3LYP						QCI					
atom or fragment	**TR**	**PR**	**1rc**	**2rc**	**3rc**	**4rc**	**TR**	**PR**	**1rc**	**2rc**	**3rc**	**4rc**
CH_2	0.07	0.11	0.26	0.24	0.23	0.23	0.07	0.11	0.24	0.23	0.23	0.23
$C(CH_2)$	−0.13	−0.12	−0.08	−0.06	−0.02	−0.05	−0.12	−0.11	−0.06	−0.04	−0.02	−0.05
$C-CH_2$	−0.06	−0.01	0.17	0.19	0.21	0.18	−0.05	0.00	0.18	0.19	0.21	0.18
C_o-H in **1**, **2** and **4**	0.03	0.00	0.08	0.06		0.04	0.02	−0.01	0.06	0.05		0.04
C_m-H in **1**, **2** and **4**	0.00	0.23	0.33	0.34		0.35	0.00	0.23	0.33	0.36		0.35
C_o in C_2H_2	−0.20	−0.24	−0.21	−0.22		−0.24	−0.20	−0.25	−0.21	−0.22		−0.24
C_m in C_2H_2	−0.24	0.01	0.06	0.08		0.09	−0.23	0.02	0.07	0.10		0.09
C_o in C_2R_2				−0.05	−0.06	−0.07				−0.06	−0.06	−0.07
C_m in C_2R_2				0.19	0.22	0.18				0.19	0.22	0.18
C_2H_2 in **1**, **2** and **4**	0.03	0.23	0.40	0.40		0.39	0.02	0.22	0.39	0.41		0.39
$C_2C_4H_4$ in **2** and **3**				0.39	0.40					0.37	0.40	
$C_2C_8H_6$ in **4**						0.42						0.42
hydrocarbon	0.05	0.46	0.80	0.79	0.79	0.81	0.04	0.44	0.79	0.78	0.79	0.81
Δ(CH) in C_2H_2	−0.03	0.24	0.25	0.29		0.31	−0.03	0.25	0.27	0.31		0.31
Δ(C) in C_2H_2	−0.04	0.25	0.26	0.30		0.33	−0.03	0.26	0.28	0.32		0.33
Δ(C) in C_2R_2				0.24	0.28	0.25				0.24	0.28	0.25
N, C_p in **T**	−0.23	−0.45	−0.30	−0.28	−0.30	−0.29	−0.22	−0.44	−0.30	−0.28	−0.30	−0.29
$H_3C(N)$, $H(C_p)$ in **T**	0.23		0.32	0.31	0.30	0.31	0.23		0.33	0.31	0.30	0.31
H_3C-N, HC_p in **T**	0.01		0.02	0.03	0.00	0.01	0.01		0.03	0.03	0.00	0.01
Me−C and N−Me			0.20	0.21	0.21	0.19			0.21	0.22	0.21	0.19

4MPR), and **1rc**−**4rc** at levels UB3LYP/6-31G* and UMP2/6-31G*, respectively. Vibrational analyses were performed for all systems at the DFT level and for **T**, **P**, **1c** and **2c** and their radicals also at the MP2 level. Bond dissociation energies BDE = $\Delta E(R-H \rightarrow R^{\bullet} + H^{\bullet})$, enthalpies $BDH_0 = \Delta(E + VZPE)$ and $BDH_{298} = \Delta(E + TE)$, and free energies $BDG = \Delta(E + TE - 298.15S)$ are summarized in Table 1, and total energies E, vibrational zero-point energies VZPE, thermal energies TE, and entropies S are reported in the Supporting Information. The QCI and CC calculations employed the 6-31G* basis set and they were based on the MP2/6-31G* structures. For systems **1** and **2** the MP2/6-31G* thermochemical data were employed to derive the respective bond dissociation enthalpies and free energies. The thermal energies and entropies used for **3** and **4** are based on the respective DFT data and scaled by the average ratios for **1** and **2**. Specifically, for the cations the scale factors for TE and S were 1.0067 and 1.0023, respectively, and for the radical cations they were 1.0298 and 0.9905, respectively.

Electron densities ρ ($\rho = \rho_\alpha + \rho_\beta$) and spin densities ρ^S ($\rho^S = \rho_\alpha - \rho_\beta$) were computed with the α- and β-densities computed at levels B3LYP/6-31G*, MP2/6-31G*, and QCI/6-31G*. The electronic and magnetic structures were analyzed by natural population analysis (NPA),[44] by inspection of surface maps (densities ρ and ρ^S, electrostatic potentials),[45] and by comparative analysis of electrostatic dipole and quadrupole moments. Tables with atomic charges q[A] for closed-shell molecules or α- and β-populations (q_α[A] and q_β[A]), total atomic charges (q[A] = AN[A] − q_α[A] − q_β[A]), and atom spin densities (q^S[A] = q_α[A] − q_β[A]) for radicals are provided as Supporting Information. Fragment charges allow for the separation of local bond polarizations from nonlocal charge shifts and pertinent data are summarized in Tables 2–5. The labels "ipso", "ortho", "meta" and "para" are used as is common for toluene, and they are also used in the same way to specify the position relative to the CH_3 group in all pyridine derivatives (rather than relative to the pyridine N atom).

TABLE 4: Electric Dipole Moments and Quadrupole Tensor Components of Toluene T, γ-Picoline P, and *N*-Methyl-γ-picolinium Cations 1c−4c, Respectively, and of the Corresponding Benzyl Radicals TR, PR, and 1rc−4rc[a]

		μ_z		μ_{tot}		Q_{zz} main axis		Q_{yy}		Q_{xx} π-density		Θ^b	
level	mol.	RH	R•	RH	R•	RH	R•	RH	R•	RH	R•	RH	R•
B3LYP	**T/TR**	0.32	−0.13	0.32	0.13	−37.82	−37.15	−38.24	−36.88	−44.81	−44.86	−4.49	−5.16
	P/PR	2.65	2.44	2.65	2.44	−43.91	−42.62	−35.97	−34.76	−43.04	−43.10	4.97	5.41
	1	−1.93	−1.11	1.94	1.11	−20.44	−18.61	−34.25	−33.23	−47.17	−47.39	5.98	5.03
	2	−1.64	−0.98	2.42	2.34	−39.82	−38.11	−41.48	−40.72	−70.77	−70.70	−20.03	−20.75
	3	−0.98	−0.65	0.98	0.70	−59.50	−57.52	−48.84	−47.76	−93.91	−94.19	−24.98	−26.50
	4	−1.54	−0.99	4.46	4.58	−59.14	−57.22	−40.36	−38.78	−94.38	−94.62	−25.12	−26.89
QCI	**T/TR**	0.28	−0.08	0.28	0.08	−38.26	−37.37	−38.51	−37.15	−45.53	−45.62	−4.76	−5.57
	P/PR	2.68	2.52	2.68	2.52	−44.76	−43.20	−36.08	−34.84	−43.73	−43.83	5.38	5.76
	1	−2.23	−1.29	2.23	1.29	−21.45	−19.35	−34.60	−33.54	−47.97	−48.26	−3.73	−5.30
	2	−1.92	−1.11	2.81	2.58	−40.70	−38.81	−42.20	−40.87	−71.99	−72.08	−20.33	−21.43
	3	−1.25	−0.57	1.25	0.65	−60.27	−57.90	−50.28	−49.75	−95.59	−95.78	−25.66	−27.16
	4	−1.79	−1.11	5.12	5.24	−59.85	−57.86	−41.36	−39.58	−96.07	−96.32	−25.96	−27.74
MP2	**T/TR**	0.29	−0.04	0.29	0.04	−38.23	−36.86	−38.50	−36.77	−45.50	−46.19	−4.75	−6.25
	P/PR	2.73	2.84	2.73	2.84	−44.85	−42.72	−36.05	−34.38	−43.70	−44.38	5.40	5.96
	1	−2.18	0.27	2.18	0.27	−21.42	−18.13	−34.44	−33.12	−47.97	−48.78	−4.91	−5.96
	2	−2.02	0.52	2.75	2.00	−40.69	−37.65	−41.89	−38.59	−71.97	−73.09	−20.43	−23.30
	3	−1.56	0.37	1.57	0.54	−60.34	−56.59	−49.30	−52.61	−95.66	−95.37	−25.64	−26.99
	4	−2.11	0.54	4.89	4.76	−60.01	−56.52	−41.08	−39.21	−95.98	−96.66	−25.68	−29.12

[a] Dipole moments in Debye (D) and quadrupole moments in Buckingham (B = DÅ). (1 au = 4.4866×10^{-40} C m^2 = 1.3450 Buckingham, B = DÅ). [b] Quadrupole moment Θ computed via $\ll\Theta\gg^3 = \Theta_{zz}^3 + \Theta_{zz}\cdot(\Theta_{xx} - \Theta_{yy})^2 = {}^4/_3\cdot(\Theta_{xx}^3 + \Theta_{yy}^3 + \Theta_{zz}^3)$.

TABLE 5: Spin Density Distributions of Benzyl Radical TR, γ-Picolinyl Radical PR, and *N*-Methyl-γ-picolinium Radical Cations 1rc−4rc

	B3LYP						QCI					
atom or fragment	**TR**	**PR**	**1rc**	**2rc**	**3rc**	**4rc**	**TR**	**PR**	**1rc**	**2rc**	**3rc**	**4rc**
CH_2	0.68	0.70	0.68	0.64	0.64	0.67	0.71	0.75	0.71	0.66	0.70	0.71
$C(CH_2)$	−0.14	−0.14	−0.08	−0.10	−0.11	−0.10	−0.19	−0.18	−0.11	−0.13	−0.07	−0.11
$C-CH_2$	0.54	0.57	0.60	0.54	0.53	0.57	0.52	0.57	0.60	0.53	0.63	0.60
C_o−H in **1**, **2** and **4**	0.21	0.21	0.14	0.19		0.18	0.24	0.22	0.15	0.22		0.18
C_m−H in **1**, **2** and **4**	−0.10	−0.09	−0.03	−0.02		−0.02	−0.13	−0.11	−0.03	−0.03		0.00
C_o in C_2H_2	0.22	0.21	0.15	0.20		0.19	0.24	0.22	0.15	0.23		0.18
C_m in C_2H_2	−0.10	−0.09	−0.03	−0.02		−0.02	−0.13	−0.11	−0.03	−0.03		0.00
C_o in C_2R_2				0.09	0.12	0.09				0.10	0.02	0.02
C_m in C_2R_2				−0.01	−0.01	−0.01				−0.02	0.07	0.04
C_2H_2 in **1**, **2** and **4**	0.11	0.12	0.12	0.17		0.16	0.11	0.11	0.11	0.19		0.18
$C_2C_4H_4$ in **2** and **3**				0.10	0.14					0.09	0.12	
$C_2C_8H_6$ in **4**						0.10						0.07
hydrocarbon	0.22	0.23	0.23	0.27	0.28	0.26	0.21	0.21	0.23	0.28	0.24	0.25
Δ(CH) in C_2H_2	−0.31	−0.30	−0.17	−0.21		−0.21	−0.36	−0.33	−0.18	−0.25		−0.18
Δ(C) inC_2H_2	−0.32	−0.31	−0.17	−0.22		−0.21	−0.37	−0.34	−0.18	−0.26		−0.18
Δ(C) in C_2R_2				−0.11	−0.13	−0.09				−0.12	0.05	0.02
N, C in **TR**	0.24	0.20	0.16	0.18	0.19	0.17	0.27	0.22	0.16	0.19	0.12	0.14
H_3C(N), H in **TR**	−0.01		0.01	0.01	0.01	0.01	−0.01		0.00	0.00	0.00	0.00
H_3C-N, CH in **TR**	0.24		0.17	0.19	0.19	0.17	0.26		0.17	0.19	0.12	0.14
Me−C and N−Me			0.77	0.73	0.72	0.74			0.77	0.72	0.76	0.75

The generation of the surface maps of spin density distributions shown in Figures 3–5 begins with the determination of an isodensity surface of the molecular electron density. We employed the same isodensity surface in all cases ($\rho = 0.04$ au). The spin density values are then determined for points on the isosurface and presented via color-coding. Regions shown in blue indicate α-spin density; those in green are relatively spin-free, and regions shown in red feature β-spin density. For the small models we also show spin density isosurfaces and these images contain the two isosurfaces with $\rho^S = +$const (α, blue) and $\rho^S =$ -const (β, green).

Calculations were performed with *Gaussian03*[46] and the magnitude of the computational task was challenging even though calculations were performed on a 64-processer SGI Altix system. The QCISD calculations of the large radicals required the option "tran = IJAB" so that the integral transformation was possible with the available disk space (ca. 1 TB) and, in fact, proceeded with a rather small disk usage (ca. 25−45 GB). Even then, some radicals were too large to compute the QCI density by the default process. The value of CONVER had to be reduced such that the convergence on the wave function was set to 10^{-6}. Control calculations with default and less-restrictive CONVER settings showed that the spin densities had converged.

The application of second-order perturbation theory to **TR**, **PR** and **1rc−4rc** does not suffice to remove the spin contaminations of the UHF reference wave functions. This is illustrated by the spin density distributions of the radicals (Figure 4) and their dipole and quadrupole moments (Table 4). Consequently, the MP2 derived BDE values of **T**, **P** and **1c−4c** are greatly overestimated and spin projection at the PMP3 and PMP4 levels is required to remedy the problem effectively (Table 1). Supporting Information is provided to document the spin contamination of the UHF wave functions and the effectiveness of its removal by increasing (a) the completeness of spin

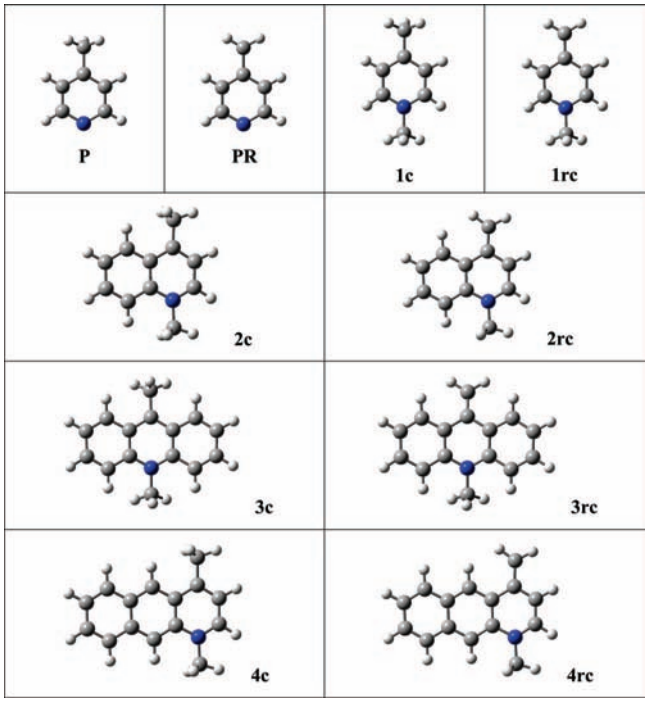

Figure 1. Molecular models of the MP2/6−31G* optimized structures of 4-methylpyridine **P** (aka γ-picoline), 1,4-dimethylpyridinium **1c** (aka 1-methyl-γ-picolinium), 1,4-dimethylquinolinium **2c**, 9,10-dimethylacridinium **3c**, 1,4-dimethylbenzo[*g*]quinolinium **4c**, and of the corresponding radical cations **PR** and **1rc**−**4rc**.

projection, (b) the order of the perturbation treatment, and (c) both of the former. We report the MP2 data in Tables 1 and 4 and in Figure 4, but no further discussion of MP2 data is provided.

Results and Discussion

Point of Reference: Benzyl Radical and Benzoannulation. The homolysis of toluene to yield benzyl radical is discussed in many textbooks of organic chemistry as the prima facie example of the energetic benefits of electron and spin delocalization (Chart 1). The hyperfine couplings in electron paramagnetic resonance (EPR) spectra inform about spin distributions,[47,48] electronic structure theory shows this spin distribution to occur by spin polarization and to feature spin alternation in most cases,[49–51] and the EPR hyperfine coupling constants are related to the electron and spin delocalization and the degree of radical stabilization.[52,53] This view of "electron and spin delocalization" permeates the research literature[54–57] and, for example, Wu et al.[57] concluded from their studies of substituent effects of neutral para-substituted toluene derivatives that "both electron-donating and electron-withdrawing groups reduce the bond dissociation energy (BDE) of the benzylic C−H bond [by 0−3 kcal/mol] because both groups cause spin delocalization from the benzylic radical center."

The bond dissociation energy of toluene has been measured by two approaches, and the agreement is excellent. In 1990, Hippler and Troe[58] reported $\Delta H_{298} = 90.4 \pm 1$ and $\Delta H_0 = 88.9 \pm 1$ kcal/mol on the basis of the measurements of the rate constants of the equilibrium $C_6H_5{-}CH_3 \rightleftarrows C_6H_5{-}CH_2^{\bullet} + {}^{\bullet}H$. In 1996, Ellison et al.[59] reported the values $\Delta H_{300} = 89.8 \pm 0.6$ and $\Delta H_0 = 88.1 \pm 0.6$ kcal/mol on the basis of their measurements of ΔG_{300} and ΔS_{300} of the gas-phase equilibrium $C_6H_5{-}CH_3 + CH_3O^- \rightleftarrows C_6H_5{-}CH_2^- + CH_3OH$, the gas-phase acidity of methanol, the electron affinity of benzyl radical, and an estimated thermal correction ($\Delta H_0 = \Delta H_{300} - 1.6 \pm 0.2$ kcal/mol). With the recent value for the gas-phase acidity of methanol[60] $\Delta G_{298} = 375.5 \pm 0.6$ kcal/mol, the derivation by Ellison et al. gives $\Delta H_{300} = 90.2 \pm 0.6$ and $\Delta H_0 = 88.6 \pm 0.6$ kcal/mol.[50a]

Benzoannulation commonly is thought to provide additional electron delocalization, (i.e., **D**, **E** and **F** in Chart 1) and, hence, additional stabilization. Finkelshtein's compilation[61] indicates bond dissociation energies of 1-methylnaphthalene (**1MN**) and 9-methylanthracene (**9MA**) that are 3.4 and 4.4 kcal/mol lower than for toluene, respectively. The compilation by Kromkin, Tumanov, and Denisov[62] also shows that the bond dissociation energies of **1MN**, **2MN**, and **9MA** are lower than for **T** by 2.4, 1.6, and 1.9 kcal/mol, respectively, but these data suggest that the bond dissociation energy of **9MA** is higher than for **1MN**. The bond dissociation energies computed at the B3LYP/4-31G level for **1MN**, **1MA**, and **9MA** are 0.7, 0.6, and 3.7 kcal/mol lower than for **T**, respectively.[63] In contrast to the available experimental data, this theoretical data would suggest that the effect of benzoannulation on the benzylic C−H bond dissociation energy is negligible.

We recently reported on studies of the effects of annulation on benzyl radical at correlated levels and determined bond dissociation energies BDH_{298} of 87.5, 88.7, 88.8, 89.7 and 84.0 kcal/mol, respectively, for the benzylic C−H bonds of **T**, **1MN**, **2MN**, **1MA** and **9MA**, respectively, at the comparable level QCISD/6-311G**//B3LYP/6-31G*.[51] The analysis of the QCI spin density of benzyl radical shows the expected α-spin densities on the ortho and para positions (Chart 1). However, this motif does not carry over to the benzoannulated systems. The spin density on the annulated ortho C atom declines in **1MNR** and the spin density closely resembles homoallyl radical and the radical **1MAR** features the electronic structure of a 2,2′-ethenylene-bridged diphenylmethyl radical (Chart 2, top). The results show in a compelling fashion that electron delocalization onto an annulated arene is *not* the decisive principle for stabilization of the benzyl radicals formed by homolysis of the polycyclic aromatic hydrocarbons $C_{10}H_7{-}CH_3$ and $C_{14}H_9{-}CH_3$. Instead, the analysis of QCI spin densities shows that electron delocalization onto annulated arenes (i.e., **D**, **E** and **F** in Chart 1) is avoided as much as possible and this is consistent with retaining a high degree of aromaticity.[64]

Roberts and Szwarc reported bond dissociation energies of 75.5, 76.5, and 77.5 kcal/mol, respectively, for α-, β- and γ-picoline, respectively,[65] relative to the bond dissociation energy of toluene which was $\Delta H_{298} = 77.5$ kcal/mol in 1948. Using $\Delta H_{298} = 89.6$ kcal/mol for the bond dissociation energy of toluene, Kromkin et al.[62] reported bond dissociation energies for α-, β- and γ-picoline of 87.2, 90.4, and 86.5 kcal/mol, respectively, and of 86.0 kcal/mol for 4-methylquinoline (**4MQ**). Hence, one realizes that the bond dissociation energies of toluene and γ-picoline are rather similar and that the effect of benzoannulation is minor in both cases.

It appears that there have been no reports of the bond dissociation energies of any of the cations **1c**−**4c**.

Symmetries and Conformations. Optimization of slightly asymmetrically deformed initial structures resulted in C_s-symmetry for all molecules (Figure 1). In **1c** and **3c**, the symmetry plane is perpendicular to the π-plane and the CH_3 groups are staggered with regard to the π-plane. This symmetry allows the two methyl groups to be staggered or eclipsed relative to each other; the former occurs in **1c** and the latter occurs in **3c**. In **2c** and **4c**, the symmetry plane coincides with the π-plane, the methyl groups eclipse each other, and one C−H bond of

CHART 1: Electron Delocalization in the Parent and Benzoannulated Benzyl Radical (Y = CH) and Their Hetero-Analogs (Y = N, NR^+)

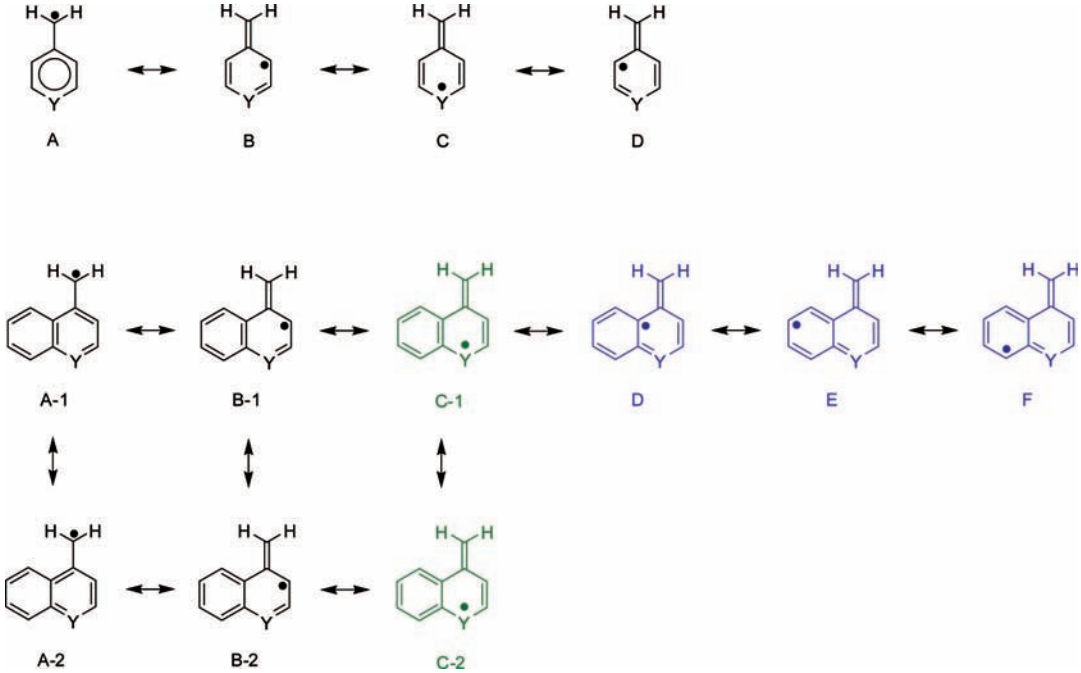

CHART 2: Avoidance of Benzyl Delocalization as Primary Stabilization Mode: Alternative Homoallyl Systems, Diphenylmethyl Systems, and Remote Spin Appearance

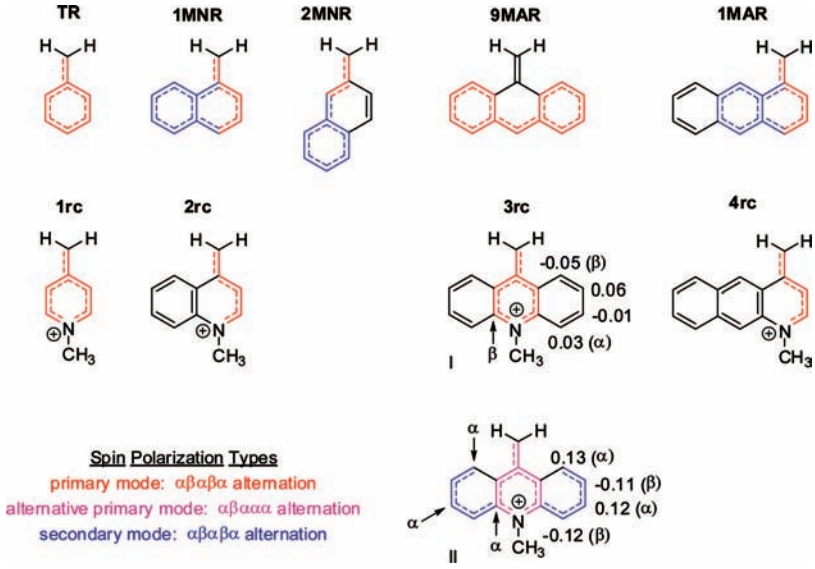

each methyl group eclipses an arene C−CH bond. Symmetries and conformational characteristics carry over to the radical cations **1rc**−**4rc**.

Homolyses of Toluene, γ-Picoline, and *N*-Methyl-γ-picolinium. Irrespective of the theoretical level, the data in Table 1 show that the bond dissociation energy of γ-picoline is just slightly higher than for toluene; BDE(**P**) > BDE (**T**). The magnitude of Δ(**P**,**T**) = BDE(**P**) − BDE(**T**) varies slightly with the method; from 1.1 kcal/mol at B3LYP to 2.3 kcal/mol at PMP4 and to 1.6−1.7 kcal/mol at the highest correlated levels. At most theoretical levels and including the best levels, the relative order of the bond dissociation energies of γ-picoline and *N*-methyl-γ-picolinium is the same, BDE(**P**) > BDE(**1c**), the difference Δ(**P**,**1c**) is below 1 kcal/mol and smaller than Δ(**P**,**T**) so that BDE(**P**) > BDE(**1c**) > BDE(**T**).

The computed bond dissociation enthalpies BDH_0 and/or BDH_{298} allow for comparisons with the experimental values $\Delta H_0 = 88.9 \pm 1$ and/or $\Delta H_{298} = 90.4 \pm 1$ kcal/mol, respectively, and unless otherwise noted we discuss BDH_{298} data. The BDH_{298}(**T**) values are 85.4−87.1 kcal/mol at the B3LYP, PMP4 and CI levels, and they are about 3−5 kcal/mol below the experimental value. This agreement is quite remarkable for homolyses and provides a first indication that the wave functions of the radicals are of high quality.

With the small difference Δ(**P**,**1c**) thermal corrections can suffice to alter the sequence of the bond dissociation enthalpies. The DFT calculations resulted in the largest value of Δ(**P**,**1c**) = 0.7 kcal/mol, and at the B3LYP level the ordering BDH_{298}(**P**) > BDH_{298}(**1c**) > BDH_{298}(**T**) remains as with the BDE data. On the other hand, the PMP4 and CI results give the ordering

BDH_{298}(**1c**) > BDH_{298}(**P**) > BDH_{298}(**T**). Most importantly, the results show very clearly that BDH_{298}(**1c**) ≈ BDH_{298}(**P**) and one gains the nontrivial insight that *N*-methylation of γ-picoline hardly effects the methyl group's C−H bond dissociation energy.

Homolyses of Annulated *N*-Methyl-γ-picolinium Ions. The DFT and MPx data show a stark theoretical level dependency of the ordering of the bond dissociation energies: The B3LYP data give the BDE ordering **1** > **2** > **4** > **3** whereas the PMP4 data suggest **2** > **1** ≈ **3** > **4**, and the most significant difference is the placement of **2**. Even after complete annihilation of all spin contaminants the PMP4 bond dissociation energy of **2** remains about 6 kcal/mol above the others. Perturbation theory is most reliable when the MPx energies converge smoothly with the order of the perturbation and this is the case for the MPx energies of the closed-shell systems **1c**−**4c** and also for the PMPx(*s*+4) energies of the radical cations **1rc**−**4rc**. Relative energies converge less smoothly and fluctuations are most pronounced for **2** (Table 1). The QCISD and CCSD energies computed for **1** and **2**, without and with triples, confirm the ordering **2** > **1** and suggest that BDE(**2**) is about 3−4 kcal/mol higher than BDE(**1**).

QCISD energies were computed for the entire series and this data results in the BDE ordering **2** > **3** > **4** ≈ **1**. Although the PMP4 and QCISD derived BDE values of **1** and **2** depend on the method, the BDE values of **3** and **4** are almost the same at both levels. It is common practice to seek higher level corroboration for small systems and to assume that the correction determined for the small systems would carry over to larger systems. As common and as accepted as it is, this practice would be seriously misleading in the present case; the higher-level calculations of the large systems *are required* and we will show why. With this CI energy data, it becomes more likely that the bond dissociation energy of **2** indeed is the highest among **1**−**4**. To fully accept this computational result requires rationales as to why **2** should be so different and, even more startling, as to why **2** should be so different from **4**.

The ordering **1** > **2** > **4** > **3** of the B3LYP bond dissociation enthalpies BDH_{298} would be expected if one followed the standard assumption that annulation would allow for more "electron and spin delocalization" and increase radical stabilities; i.e., benzoannulation is good, naphthoannulation is better, and double annulation is better than single annulation. In contrast, the PMP4 and QCI data result in the relative BDH_{298} ordering **2** > **3** > **4** > **1** and suggest that the annulations increase the bond dissociation energies and result in a nontrivial ordering. Analyses of electronic structures and spin density distributions have been performed to elucidate the many similarities and the few, but significant differences between the DFT and QCI results.

Electronic Relaxation in γ-Picolinium Homolyses. Toluene is nonpolar (charges on all CH groups, C_{ipso} and the CH_3 group are less than 0.05) and CH/N replacement causes strong but local C−N bond polarizations in γ-picoline (Table 2). In γ-picolinium ions **1c**−**4c**, the N atom remains negatively charged by $q(N) \approx -0.3$, the *N*-methyl group's positive charge is about equal in magnitude, leaving the NCH_3 group *almost neutral* (Chart 3). Across the ring, the C_{ipso} atom is slightly positive $q(C_{ipso}) \leq 0.1$, its CH_3 is electron-deficient with $q(CH_3) \approx 0.1$, and the C−CH_3 fragment overall is positive by about 0.2. Thus, about *80% of each ion's charge is associated with C_2H_2, $C_2C_4H_4$, and $C_2C_8H_6$ fragments* and, moreover, the charge is about equally distributed over both "arms" connecting N and C_{ipso} in **1c**−**4c**.

The homolyses of nonpolar **T** and of locally polar **P** cause some polarity in the C_{ipso}−CH_2 regions of **TR** and **PR** (Table 3). The same kind of C_{ipso}−CH_2 polarization occurs during the homolyses of **1c**−**4c** albeit the result is slightly different: The C_{ipso}−CH_3 fragments are slightly positive in **1c**−**4c**, they remain positive in **1rc**−**4rc**, and the regions become bipolar.

The positive charge of the C_m−H/R fragments in the pyridines and polarization within overall near-neutral C_o−H/R fragments causes C_o−C_m bond polarities and these are characterized by the $\Delta(C) = q(C_o) - q(C_m)$ values. Compared to **1c**, annulation in **2c** and **4c** reduces the shared bonds' polarities and increases the unshared C_o−C_m bonds' polarities more, and in **3c** both shared bonds are more polar than in **1c**. The C_o−C_m bond polarities all are reduced during the homolyses of **1c**−**4c**, and the reductions are more pronounced for the more polar bonds. For an annulated bond, any decrease of its polarization would tend to improve the fused arene's aromaticity. One might thus wonder about possible correlations with the bond dissociation energies of **1c**−**4c**. Yet, the homolysis of **3c** is slightly more difficult than for **1c** even though the arenes in **3rc** become more aromatic in the process (vide infra) and this line of argument alone also does not lead to a consistent rationale of the relative dissociation energies of **2c** and **4c**.

Electrostatic Potentials and Molecular Moments. Molecular electrostatic characteristics are observable properties and inform about the adequacy of the computed electron density distributions. Furthermore, changes in these properties upon homolysis can be connected to the analysis of electronic effects. Computed electrostatic potentials are shown in Figure 2, and dipole moments μ_{tot} and μ_z in Debye (D) and quadrupole moments Q_{zz} in Buckingham (B = DÅ) are reported in Table 4. The molecules are aligned such that the C_{ipso}−CH_n bonds coincide with the *z*-axis and that the π-plane coincides with the *xy*-plane as best as possible (or exactly). The deviations between μ_z and μ_{tot} for **2** and **4** shows substantial polarization of the fused arenes by the γ-picolinium core.

The computed dipole moment of toluene agrees with experiment (0.38 D).[66] The reversal of the direction in benzyl radical had been noted[67] and is reproduced at the DFT ($\Delta\mu_z = -0.45$ D) and QCI ($\Delta\mu_z = -0.36$ D) levels. The direction of the dipole moment of **T** is caused by σ-π interaction between CH_3 density and arene π-density.[68] Homolysis removes this electron−electron repulsion and leads to arene π-density polarization in the opposite direction. The directions of the dipole moments of **P** and **PR** are in sync with the CN bond polarities (Chart 3), the computed values compare to the dipole moment of pyridine,[69] and their high magnitudes stress the importance of the pyridine-N's lone pair moment.[70] As with toluene and for the same reason, the homolysis of γ-picoline is accompanied by a reduction of the dipole moment by $\Delta\mu_z = -0.21$ (DFT) and $\Delta\mu_z = -0.16$ (QCI).

The directions of the dipole moments of **1c** and **1rc** are opposite to those of **P** and **PR** because the N−CH_3 polarity is opposite to the N lone pair polarity. The population data show similar C_{ipso}−CH_n polarization relaxations for the homolyses of **T**, **P** and the picolinium systems, and the data suggest an additional change in the same direction due to C_o−C_m polarization relaxations during the homolyses of **P** and **1c**−**4c**. The corresponding changes of the molecular dipole moments (i.e., μ_z becomes more positive/less negative) are overwhelmed by the changes of the intramolecular polarization of **T** and **P** during their homolyses. Intramolecular polarization related to σ-π interaction is much less important in the cationic systems,[71,72] and the dipole moments of the picolinium systems do become

CHART 3: Polarities of Toluene T, γ-Picoline P, and *N*-Methyl-γ-picolinium 1c and Their Homolysis Products Benzyl TR, γ-Picolinyl PR, and *N*-Methyl-γ-picoliniumyl 1rc, Respectively

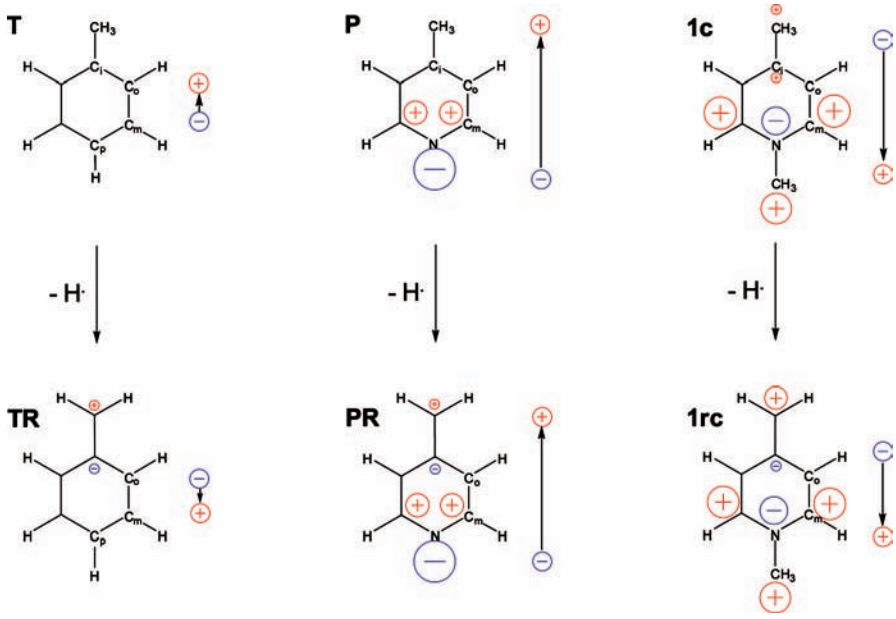

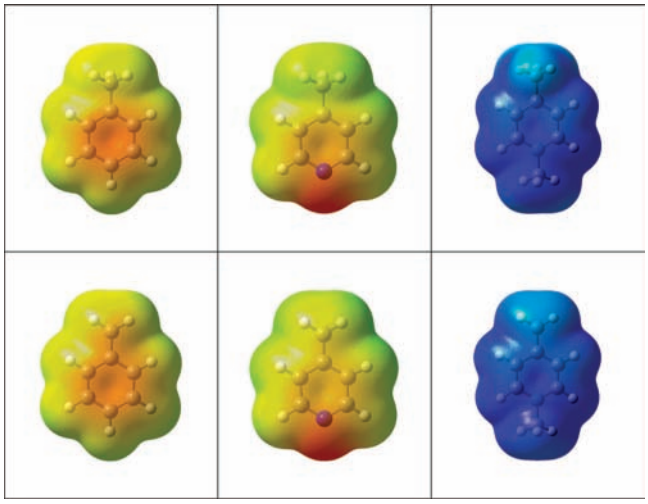

Figure 2. Electrostatic potentials of toluene **T** and benzyl radical **TR** (left), of 4-methylpyridine **P** and 4-methylpyridinium-4-yl **PR** (center), and of 1,4-dimethylpyridinium **1c** and 1,4-dimethyl-pyridinium-4-yl **1rc**. The QCI/6-31G*//MP2/6-31G* potentials are shown, their values are color-coded (−0.05 to +0.15 au), and they are displayed on isosurfaces of the electron densities ($\rho = 0.0004$ au).

more positive; $\Delta\mu_z$(DFT) +0.82 (**1**), +0.66 (**2**), +0.33 (**3**), and +0.55 (**4**); $\Delta\mu_z$(QCI) +0.94 (**1**), +0.81 (**2**), +0.68 (**3**), and +0.68 (**4**).

The quadrupolarity of aromatic systems is receiving increasing attention and many of the parent aromatic and heteroaromatic systems have been well characterized.[73] Much less is known about the quadrupolarity of substituted and/or charged systems and of the molecules discussed here only the quadrupole moment of **T** has been measured; $\Theta(T) = -7.92$ B.[74,75] The quadrupole moment Θ has the quality of a *quadrupole moment tensor anisotropy*, represents the (effective) axial quadrupole moment, and is related to the traceless quadrupole moment tensor components Θ_{ii} via $\Theta = {}^4/_3(\Theta_{xx}{}^3 + \Theta_{yy}{}^3 + \Theta_{zz}{}^3)$. The traceless quadrupole tensor components Q_{ii} in turn are constructed from the unabridged quadrupole tensor components Q_{ii}, and the latter are computed directly from the electron density distribution (Table 4).[76] By definition, the quadrupole moment tensor components Q_{ii} are sensitive to the description of diffuse electron density, to reach convergence of the Θ_{ii} values is harder, and the precise determination of the sign and value of the quadrupole moment Θ can be extremely difficult.[76] For **1c** and **1rc**, for example, one Θ_{ii} component is close to zero and the others are of about equal magnitude and different sign; a perfect storm for small differences in Q_{ii} to become magnified in Θ.

We are interested in Q_{zz} (Table 4) because this tensor component provides information about the polarity relaxation in the $C_{ipso}-CH_n$ regions. The quadrupole moment values Q_{zz} of **T** and **P** are negative and N-methylation reduces the value by more than 50% to about −20 B (but Q_{zz} remains negative), and each fused arene contributes roughly an additional −20 B to Q_{zz}. The data show that C−H bond dissociation increases the quadrupole moment tensor components Q_{zz} (*less* negative) as the radical is formed. This finding is independent of the theoretical level and applies to all cases studied. This computational result provides evidence in support of the polarization of the $C_{ipso}-CH_n$ regions upon homolysis of the cationic *and* of the neutral systems.

Spin Polarization: Mechanisms and Outcomes. "Spin polarization" (SP) refers both to the *mechanisms* and to the *effects* of spin−spin interactions. Effects of spin polarization are the electronic and magnetic features of the total electron density that result from the interaction of an unpaired α spin electron with all other electrons in the molecule. Although spin polarization enters naturally in valence bond (VB) theory,[26] the ubiquitous single-determinant restricted LCAO-MO theory (ROHF, EHT, Hückel) neglects any and all spin polarization and in this approximation the electron density distribution of the singly occupied HOMO (SOHOMO) is said to inform about "electron and spin delocalization". Actual, spin-polarized spin density distributions[77−79] often feature SOHOMO-like spin distributions with αβ-alternations of spin populations of the atoms along the molecular skeleton, and methyl,[77] allyl,[78] and benzyl[51] are important and well-studied prototypical radicals. To think about the spin densities of these prototypes in terms of "electron and spin delocalization" does not create obvious conflicts.

CHART 4: Spin Dipole and Spin Quadrupole Polarizations in Localized and Delocalized MOs

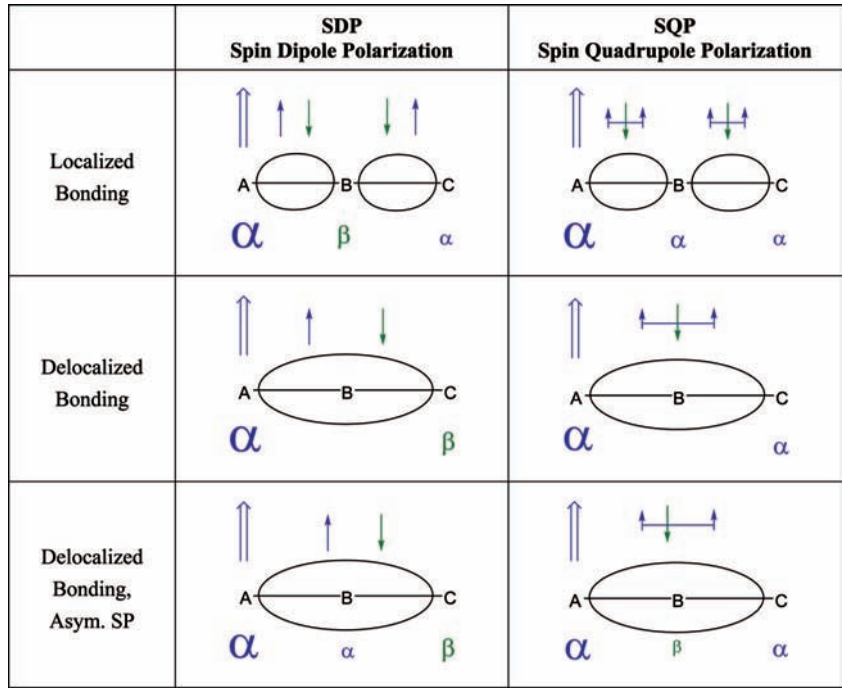

It is useful to develop a conceptional understanding of the mechanisms of spin polarization so that one can formulate expectations without prejudice (Chart 4). Given an atom A that carries unpaired α-spin density (⇒) and functions as SP-originator, we consider the effects of spin polarization on "electron pairs" that involve atom A. The quotes are used because every doubly occupied ROHF-type MO has been replaced by a product $\rho^{\alpha}(1)\rho^{\beta}(2)$ of two singly occupied spin molecular orbitals (SMO). Up and down arrows (↑, ↓) indicate the centers of α- and β-spin in the $\rho^{\alpha}(1)\rho^{\beta}(2)$ spin density and $\alpha\beta$-spin dipole polarization (SDP) is the simplest possibility (↑, ↓). The unpaired electron causes $\alpha\beta$-SDP of a localized pair density (top-left) and results in more same-spin electron density (localization) in the vicinity of atom A and β-spin density appears at atom B. In turn, the β-spin density at atom B may cause α-spin density to appear at atom C. The resulting spin populations at atoms B and C, respectively, correspond to the first- and second-order contributions considered by Adamo et al.[50] and these authors emphasized that "spin density due to the second-order terms will generally be smaller". In unsaturated molecules some occupied MOs are delocalized and the associated electron pairs allow for spin polarization across two bonds (Chart 4, left, center and bottom). Depending on the positions of the centers of spin density relative to atom B, such 1,3-$\alpha\beta$-SDP may occur essentially without (left-center) or with significant (left-bottom) spin density accumulation at atom B.

The $\alpha\beta$-spin dipole polarization is not the only possibility and there are compelling reasons to consider $\alpha\beta\alpha$-spin quadrupole polarizations (SQP) in localized and delocalized "electron pairs". The O_2 molecule[80] was shown to feature $\alpha\beta\alpha$-SQP, for example, and the principle might best be understood considering the familiar π-MOs of allyl radical (Chart 5). Allyl's unpaired π_2^{α}-electron places α-spin density on both methylene C atoms and each α-spin density basin seeks to polarize the $\pi_1^{\alpha}(1)\pi_1^{\beta}(2)$-density so as to increase α-spin at *both* methylene ends. This physically desired outcome is accomplished by variation of the relative contributions of the $p_{\pi}(CH_2)$ and $p_{\pi}(CH)$ contributions to π_1^{α} and π_1^{β}, respectively, and the $\alpha\beta\alpha$-SQP of the $\pi_1^{\alpha}(1)\pi_1^{\beta}(2)$-density should be no surprise. SQP has significant consequences on the long-range spin density distribution and these are illustrated in the right column of Chart 4. In general, to deform a dipole into a quadrupole requires the replacement of at least one monopole by a pair of same-type monopoles. In Chart 4, the quadrupolarity of the spin density is illustrated by the occurrence of two centers of α-spin density for each α-spin−orbital and symbolized by a pair of smaller up arrows (↑—↑).

CHART 5: Spin Quadrupole Polarization of Allyl's "π_1-Electron Pair" by the Unpaired Electron in the π_2-SMO

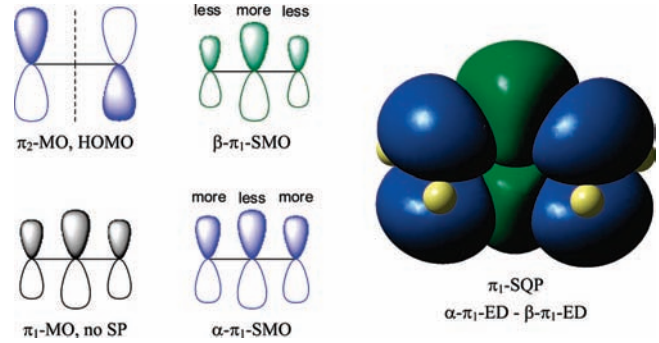

The use of the term "spin delocalization" is somewhat unfortunate in that spin polarization always increases same-spin density in the immediate vicinity of the SP-originating spin (atom A in Chart 4) and usually also increases the spin population of atom A. Second-order SDP creates same-spin elsewhere by concentration of spin at the originator and the resulting $\alpha\beta$-alternation; *not* by distribution of the originator's spin. And SQP also does not affect genuine delocalization. Nevertheless, spin polarization of delocalized "electron pairs" $\rho^{\alpha}(1)\rho^{\beta}(2)$ can have the effect of delocalizing spin density from one atom's region into another atom's region if the spin polarization creates asymmetries as illustrated in the bottom row

of Chart 4. SQP can result in a decrease of α-spin density in region of atom A if the β-density is asymmetrically distributed with more β-density in the AB region than in the BC region; α-spin density has effectively been delocalized away from atom A.

The widely held assumption that spin polarization simply alters an atom's spin population one way or the other is another misconception. Instead, spin polarization might create β-spin regions in the atomic basins of atoms that carry α-spin even as the overall α-spin population of that atom increases. A few simple examples of spin polarization are illustrated in Figure 3. The methyl radical (CH_3, $^2A_2$) serves as the familiar reference and illustrates the typical SDP-type spin polarization of the C−H bonds by the unpaired p_z-electron. The radical cations of ethene ($C_2H_4^+$, $^2B_{2u}$) and acetylene ($C_2H_2^+$, ^2B_u) exemplify the case of a π^1 radical, that is, a radical with directly adjacent and equal SP-originating atoms, and the spin polarizations of the C−H bonds again are of the typical SDP-type. Note, however, the occurrences of the thin discus-shaped and the flattened hourglass-shaped regions of β-spin density in the centers of the C−C bonding regions of the cations, respectively, and these features are the result of SQP-type spin polarization. If the two SP-originating atoms are only attached to each other, then all the spin polarization has to occur in their basins and much larger effects occur in the bonding regions. This situation is illustrated by the σ^1-radical cation of dinitrogen (N_2^+, $^2\Sigma_g$) and the oxygen triplet diradical ($^3O_2$, $^3\Sigma_g$). The β-spin region in the N−N bonding region of N_2^+ occupies the space of a hollow conical cylinder. The O_2 molecule features two kinds of intensive β-spin appearances, and they are symmetric about O_2's main axis; a large β-spin region appears between the atoms in the shape of a red blood cell and two pear-shaped regions extend into the cone cap regions.

These concepts can be applied to unsaturated radicals by considering the combined effects of all SP-originators and their locations are provided by the shape of the SOHOMO. Allyl radical, for example, contains two equal SP-originators. The situation becomes more complex for a radical with a delocalized SOHOMO with several unique SP-originators, and we discuss benzyl and its analogues as case studies.

Spin Densities of Benzyl, γ-Picolinyl, and γ-Picoliniumyl. The spin density distributions of **TR**, **PR** and **1rc** are shown in Figure 4, and spin populations are given in Table 5. The DFT and QCI spin density distributions are qualitatively similar and show αβ-spin alternation; α-spin is located in the CH_2-, C_o- and C_p-regions and small β-spin densities appear around the C_{ipso}- and C_m-atoms. The MP2 spin densities exemplify the drastic consequences of spin contaminations.

The spin populations show that **TR**, **PR** and **1rc**−**4rc** have 70 ± 5% of one α-spin on the CH_2 group, some β-spin at C_{ipso}, and spin populations of 0.58 ± 0.05 in their C_{ipso}−CH_2 regions. **TR** and **PR** feature about equal amounts of α-spin populations on the C_oH and Y fragments (C_pH or N) and roughly half as much β-spin population on the C_mH fragments. The α-spin populations of the C_oH and Y fragments in **1rc** are smaller than in **PR** and the β-spin populations on the C_mH fragments are merely one-fifth of the α-spin populations of adjacent fragments.

The effects of electron correlation on electron and spin density distributions are exemplified by comparison of the ROHF and QCI data of **TR**, **PR**, and **1rc** in Chart 6. The changes of the electron density in the C(CH_2)-region are small and electron correlation moves electron density *into* the region. On the other hand, there are large decreases of α-spin density in the C(CH_2)-regions. Electron correlation certainly does not promote electron

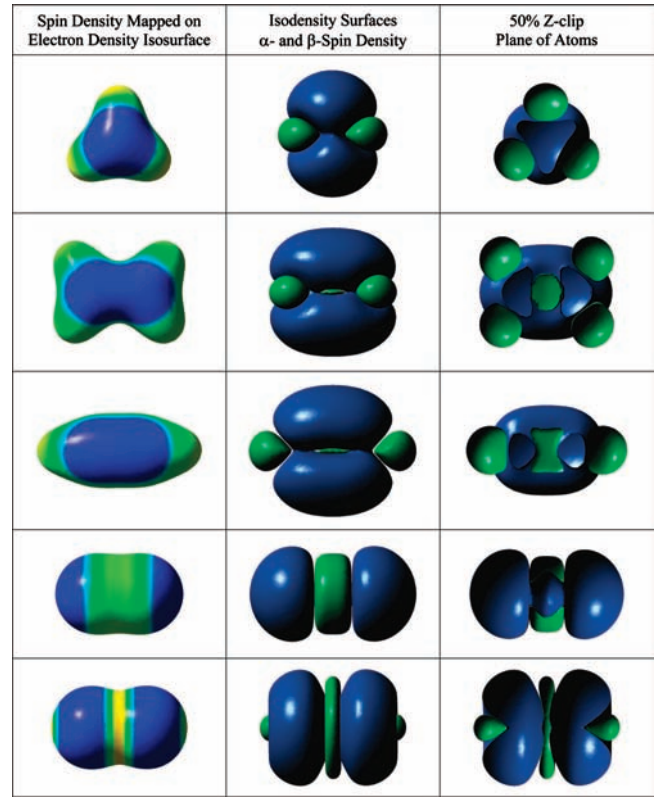

Figure 3. Spin polarization in (from top) methyl radical (CH_3, $^2A_2$), radical cations of ethene ($C_2H_4^+$, $^2B_{2u}$), acetylene ($C_2H_2^+$, ^2B_u), and dinitrogen (N_2^+, $^2\Sigma_g$), and triplet oxygen ($^3O_2$, $^3\Sigma_g$). Electron density isosurface for $\rho = 0.04$; spin density isosurfaces for $\rho^S = \pm 5 \times 10^{-4}$.

delocalization away from the site of the largest concentration of unpaired spin, but electron correlation does cause α-spin delocalization away from the dominant SP-originator (SPO1). This "spin-only delocalization" does not result in a more even distribution of α-spin but instead comes with larger increases of α-spin at the locations of the minor SP-originators (C_o, Y). The notion of "the one delocalized α-spin electron" has to be abandoned in the discussion of actual, correlated densities. Electron correlation causes an overall increase of α-spin regions and β-spin appearance elsewhere. Instead of a nonmagnetic electron density distribution containing a few spikes of really large α-spin density, electron correlation creates a heavily spin-polarized electron density in which the largest centers of α-spin density are reduced.

The data in Chart 6 show a rough inverse relationship between the size of the correlation effects on electron and spin densities. Correlation effects on the electron density distribution of nonpolar **TR** are small and changes to the spin density are largest, and vice versa for polar **1rc**.

Shared Bond Spin Polarization in Annulated γ-Picoliniumyls. The DFT and QCI spin density distributions of the annulated picoliniumyls **2rc**−**4rc** are shown in Figure 5. On first examination the spin density distributions ρ^S(**2rc**) and ρ^S(**4rc**) appear qualitatively similar at both levels whereas ρ^S(**3rc**) exhibits obvious differences. Common to **2rc** and **4rc** is the feature that electron and spin delocalization onto the annulated arene is quite unimportant, and in fact, the shared bonds of these monoannulated picoliniumyl systems are almost spin-free.

The methodological differences for **3rc** striking. DFT results in a **1rc**-like spin density for the core moiety of **3rc**, and in a

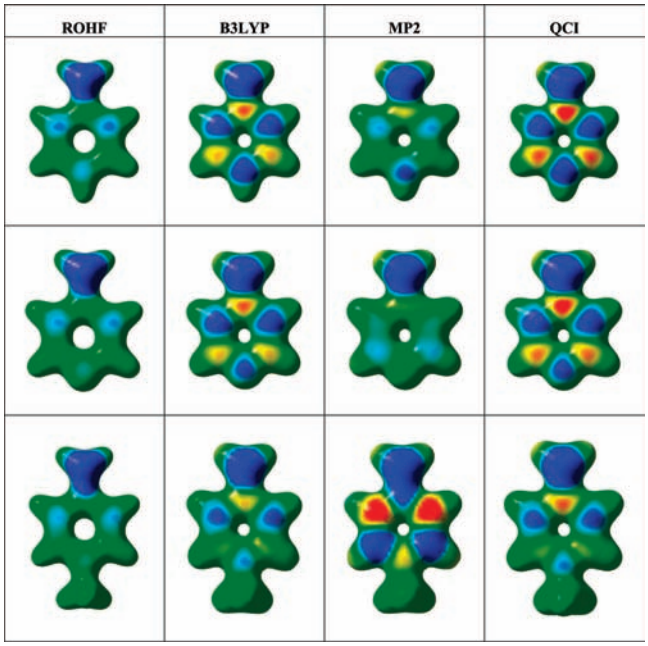

Figure 4. Spin density distributions of benzyl radical and its pyridine and pyridinium derivatives. Spin densities are color-coded (-4.432×10^{-3} to 4.432×10^{-3} au) and displayed on isosurfaces of the electron densities (value 0.04 au).

CHART 6: "Electron Delocalization" and "Spin Delocalization" in the Regions C(CH$_2$), C$_o$H, C$_m$H, and Y[a]

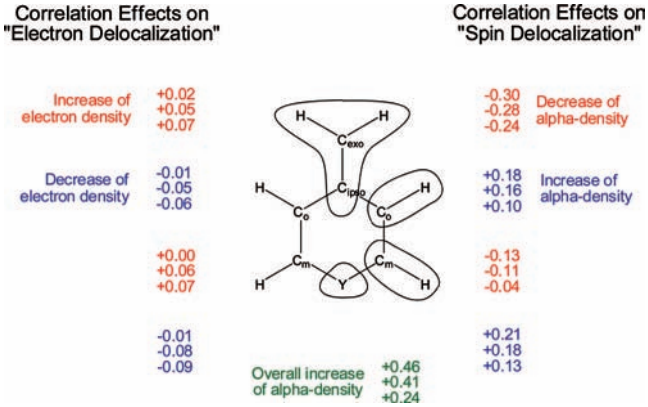

[a] Each set contains data for **TR** (Y = C$_p$H), **PR** (Y = N), and **1rc** (Y = NCH$_3$) on differences between ROHF and QCI data.

feeble attempt to *minimize the perturbation of the annulating arenes*, the α-spin of the C$_o$ atoms is decreased whereas the α-spin on the C$_p$ atom is increased. QCI changes the game entirely: the electronic structure of the "annulated γ-picoliniumyl core" is abandoned in favor of an electronic structure that *minimizes the perturbation of the central heteroarene* (much less than in **PR**) and spin density appears in the annulating arenes. Radical **3rc** truly stands out among **1rc**−**4rc** because it features the most localized methyl radical and the least α-spin population on the NCH$_3$-fragment. The electronic structure of the PAH analog **9AR** also was found to be special but for another reason. The high stability of **9AR** is due to the formation of the diphenylmethyl radical electronic structure. In contrast, there is no advantage for the adoption of a diphenylaminiumyl electronic structure in **3rc**.

The shared bond regions in **1rc** and **2rc** are α(C$_o$)β(C$_m$) spin-polarized and each "homoallyl" chain features the αβαβα spin pattern, i.e., α(CH$_2$)β(C$_{ipso}$)α(C$_o$)β(C$_m$)α(N). However, the shared bond regions in **3rc** and **4rc** become α-spin regions with higher α-spin populations on the C$_m$ atoms, the αβααα spin pattern α(CH$_2$)β(C$_{ipso}$)α(C$_o$)α(C$_m$)α(N) occurs. This feature remains relatively inconsequential in **4rc**, but the α(C$_m$)-spins make possible the αβ-spin alternation along the periphery of **3rc**.

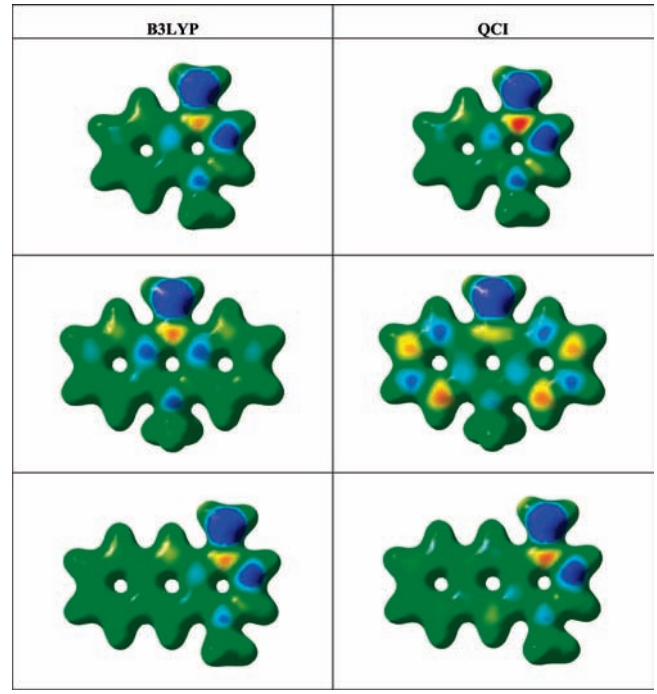

Figure 5. Annulation effects on spin density distributions of radical cations **2rc**−**4rc** computed with the B3LYP/6-31G* and QCI/6-31G* densities. Spin densities are color-coded (-4.432×10^{-3} to $+4.432 \times 10^{-3}$ au) and displayed in isosurfaces of the electron densities (value 0.04 au).

DFT and QCI spin populations (Table 5) show the same qualitative features for **1rc**, **2rc**, and **4rc** but diverge as to whether **3rc** fits in (DFT) or stands out (QCI). Spin populations of peripheral CH groups are given in Chart 2 in light of the DFT (**I**) and QCI (**II**) results. Radicals **2rc** and **4rc** feature higher α-spin population on their remaining C$_o$H region compared to **1rc** (q^s(C$_o$H): 0.15 (**1rc**), 0.22 (**2rc**), 0.18 (**4rc**)), diverging behavior in their Y-fragments (q^s(NCH$_3$): 0.16 (**1rc**), 0.19 (**2rc**), 0.14 (**4rc**)), and greatly reduced spin densities on the shared bonds and/or the fused arene. Hence, the spin density distributions show **2rc** and **4rc** to be "homoazaallyl" radicals with slightly more emphasis on the "allyl" part in the case of **4rc**.

Breakdown of SOHOMO-Based Rationalization of Spin Density Distributions. The resonance forms in Chart 1 describe *electron delocalization* in VB terms and knowing their relative contributions provides information that is equivalent to the knowledge of the shape of the SOHOMO in MO theory. Although the resonance structures of Chart 1 cannot fully inform about the *spin density distribution*, they often provide qualitative information. In the present case, the DFT spin densities could be interpreted to reflect a preference for contributions of **A**-, **B**- and **C**-structures over **B**- and **D**-structures and disadvantages for contributions of **E**- and **F**-structures. A cursory analysis of the QCI spin densities might indicate preferences of the **A**- and **C**-structures with contributions from all others (**B**−**F**) greatly diminished. Yet, comprehensive analysis shows that the QCI spin densities of **3rc** and **4rc** are incompatible with the SOHOMO-based approach. Again, it is emphasized that the QCI electronic structure of **3rc** must not be confused with the

CHART 7: Strategies To Control the Stabilities and Reactivities of *N*-Alkyl-γ-picoliniumyl Radicals Aim at the Manipulation the C_o-C_m Bond Polarity

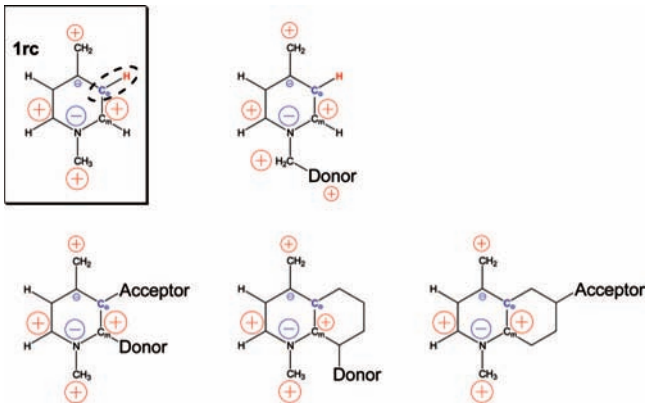

"diphenylmethyl radical" nature of **9AR**. The α-spin locations in the annulating arenes of **9AR** happen to coincide with the locations of the unpaired electron in structures **F** and **E**; those in **3rc** do not.

The SOHOMO-based rationalization is applicable only if the topology of the spin-originators remains unchanged by electron correlation. Even though the topology of the spin originators is retained in many radicals (including the benzyl-type radicals **TR**, **PR**, and **1rc**, and the annulated derivatives of benzyl radical[51]), there is no reason to suggest that it must. The spin density distributions of **3rc** and **4rc** show that the topology can change, and **3rc** shows that the change in topology can have molecule-wide consequences.

Bond Dissociation Energies and Electronic Structures. The comparative analysis of the DFT and QCI data show a great many similarities. Toluene is nonpolar and γ-picoline features local C−N polarities, and both substrates feature essentially neutral $C_{ipso}-CH_2$ moieties. The *N*-methyl-γ-picolinium ions feature positive charges on both the C_{ipso} atom and the CH_2 group. The homolyses of the neutral radicals are mostly local events as far as their electron density distributions are concerned and lead to bipolar $C_{ipso}-CH_2$ moieties. The homolyses of the γ-picolinium ions also result in bipolar $C_{ipso}-CH_2$ groups, but it is an additional and distinguishing feature of these cationic substrates that their homolysis also increases the C_o-C_m bond polarities. Annulation provides resistance to polarity increases in shared C_o-C_m bonds to maintain the arene's aromaticity as much as possible. There also is general agreement that spin polarization causes the delocalization of α-spin onto the ortho (C_o) and para-positions (C_p, N_p) and that the spin delocalization onto the para-position is significantly reduced in the γ-picolinium systems.

The DFT and QCI data also agree that the effects of annulation on the bond dissociation energies are modest even though the methods place **1** high or low, respectively. The most significant difference between the methods concerns the placement of the bond dissociation energies of **3** and **4**, and this difference is caused by their different spin polarizations. The electronic effects of annulation on C_o-C_m bond polarity provide a strong rationale for the increase of the bond dissociation energies of **2**−**4** relative to **1** at the QCI level. This effect would suggest the ordering **3** > **4** ≈ **2** > **1** whereas the actual BDE ordering is **2** > **3** > **4** ≈ **1** at the QCI level. Hence, there has to be an additional mechanism that stabilizes **3rc** and **4rc** more than **2rc**. Our analysis of the spin densities shows that **1rc** and **2rc** feature the αβαβα spin pattern in each of their two homoallyl chains, whereas **3rc** and **4rc** realize αβααα spin patterns along the chains that include shared bonds. We suggest that it is this feature that distinguishes **4rc** from **2rc**. The αβααα spin pattern of **3rc** and **4rc** make possible the spin appearance in the periphery and, lacking any other form of stabilization, **3rc** actually shows spin appearance.

Conclusion

The spin density distributions cannot be understood, not even qualitatively, without the consideration of spin polarization. The adequate description of such long-distance effects requires a method that accounts well for dispersion. The DFT calculations miss at least some of these effects, and it is for this reason that we consider the QCI results to provide the most trustworthy results. As with the annulated benzyl radicals, in the annulated picoliniumyl radicals the extent of spin delocalization into annulated arenes is kept *as low as possible*. Electron and spin delocalization into an arene comes at a cost because spin polarization reduces aromaticity.[64] Although molecule-wide spin polarization occurs with spin alternation in annulated benzyl radicals, molecule-wide effects are greatly reduced in the annulated picoliniumyl radicals and occur only if there is no alternative. Radical **3rc** features peripheral spin appearance.

The calculated bond dissociation energies show that *N*-methyl-γ-picoliniumyls **1c**−**4c** are on par with the radicals **TR** and **NR** regarding their capabilities for hydrogen abstraction and radical addition. However, there is a major difference in the way this reactivity is delivered and the charge and the polarity provide advantages for the interactions of the γ-picoliniumyls with DNA.

Overall, the sort of careful analysis presented here has the potential to facilitate the design and understanding of antitumor agents whose actions depends upon radical intermediates. The analysis suggest several strategies to alter the stabilities and reactivities of the radicals and these aim at the manipulation the C_o-C_m bond polarity without impeding the reactive methylene group. The fragment charges of **1rc** are shown in Chart 7 and it is indicated that the C_o-H bond is polar even though the C_oH fragment is almost neutral. The first strategy aims to reduce the primary cause for the C_o-C_m bond polarity and consists in the replacement of the *N*-methyl group with groups that move the positive charge further away from the heteroarene. The second strategy accepts the fundamentals of the *N*-methyl-γ-picoliniumyl system and aims at the manipulation of the C_o-C_m bond polarity by acceptor (e.g., F, Cl, C≡N, C≡CR, ...) and/or donor (e.g., alkyl, alkoxy, phenyl, phenoxy, ...) substitution. The substitution at C_o is interesting as it allows for the simultaneous manipulation of the electron and the spin densities. The cyano group would seem to be a good candidate for this position as it is a strong acceptor and capable of effective spin delocalization. If one wanted to alter mostly the spin distribution, one might place less electronegative and spin-polarizing groups (C≡CR, phenyl) at the C_o position. The third approach is a variation of the second for annulated systems and the perturbations are applied to the fused arenes.

Acknowledgment. We thank Drs. Gordon Springer, Larry Sanders, and Slava Zagrzewki for their assistance and advice about hardware and software issues. Dr. Alexander Safronov kindly translated relevant Russian papers. Funding by the MU Research Board (RB #2358) and the National Institutes of Health (CA 100757) contributed to this work. MU Research Computing

is supported by Federal Earmark NASA Funds for Bioinformatics Consortium Equipment and additional support from Dell, SGI, Sun Microsystems, TimeLogic and Intel.

Supporting Information Available: Details of the potential energy surface analyses (Cartesian coordinates, total energies E_{tot}, thermal energies TE, thermal entropies S) and of the electronic structure analyses (atom charges q, atom spin populations q^S), and results of spin projection calculations up to PMP4(s+4). This material is available free of charge via the internet at http://pubs.acs.org.

References and Notes

(1) Bagley, A. C.; Krall, J.; Lynch, R. E. *Proc. Natl. Acad. Sci. U.S.A.* **1986**, *83*, 9189–9193.

(2) Hassan, H. M.; Fridovich, I. *Arch. Biochem. Biophys.* **1979**, *196*, 385–395.

(3) Sanchez Sellero, I.; Lopez-Rivadulla Lamas, M. *Recent Res. Dev. Drug Metab. Disp.* **2002**, *1*, 275–313.

(4) Hassan, H. M.; Fridovich, I. *J. Bacteriol.* **1980**, *141*, 156–163.

(5) Denny, W. A. *Lancet Oncol.* **2000**, *1*, 25–29.

(6) Brown, J. M. *Cancer Res.* **1999**, *59*, 5863–5870.

(7) Sies, H. *Angew. Chem., Int. Ed. Engl.* **1986**, *25*, 1058–1071.

(8) Elwell, J. H.; Siim, B. G.; Evans, J. W.; Brown, J. M. *Biochem. Pharmacol.* **1997**, *54*, 249–257.

(9) Wouters, B. G. *Cancer Res.* **2001**, *61*, 145–152.

(10) Lloyd, R. V.; Duling, D. R.; Rumyantseva, G. V.; Mason, R. P.; Bridson, P. K. *Mol. Pharmacol.* **1991**, *40*, 440–445.

(11) Patterson, L. H.; Taiwo, F. A. *Biochem. Pharmacol.* **2000**, *60*, 1933–1935.

(12) Anderson, R. F.; Shinde, S. S.; Hay, M. P.; Gamage, S. A.; Denny, W. A. *J. Am. Chem. Soc.* **2003**, *125*, 748–756.

(13) Daniels, J. S.; Gates, K. S. *J. Am. Chem. Soc.* **1996**, *118*, 3380–3385.

(14) Birincioglu, M.; Jaruga, P.; Chowdhury, G.; Rodriguez, H.; Dizdaroglu, M.; Gates, K. S. *J. Am. Chem. Soc.* **2003**, *125*, 11607–11615.

(15) Kotandeniya, D.; Ganley, B.; Gates, K. S. *Bioorg. Med. Chem. Lett.* **2002**, *12*, 2325–2329.

(16) Daniels, J. S.; Gates, K. S.; Tronche, C.; Greenberg, M. M. *Chem. Res. Toxicol.* **1998**, *11*, 1254–1257.

(17) Hwang, J.-T.; Greenberg, M. M.; Fuchs, T.; Gates, K. S. *Biochemistry* **1999**, *38*, 14248–14255.

(18) Marcu, L.; Olver, I. *Curr. Clin. Oncol.* **2006**, *1*, 71–79.

(19) Sundararajan, C.; Falvey, D. E. *J. Org. Chem.* **2004**, *69*, 5547–5554.

(20) Falvey, D. E.; Sundararajan, C. *Photochem. Photobiol. Sci.* **2004**, *3*, 831–838.

(21) Riordan, C. G.; Wei, P. *J. Am. Chem. Soc.* **1994**, *115*, 2189–2190.

(22) Zady, M. F.; Wong, J. L. *J. Org. Chem.* **1980**, *45*, 2373–2377.

(23) Mohler, D. L.; Shell, J. R.; Coonce, J. G.; Mirandi, J. L.; Riera, L.; Cuesta, L.; Perez, J. *J. Org. Chem.* **2007**, *72*, 8755–8759. (b) Mohler, D. L.; Downs, J. R.; Hurley-Predecki, A. L.; Sallman, J. R.; Gannett, P. M.; Shi, X. *J. Org. Chem.* **2005**, *70*, 9093–9102.

(24) Russell, G. A.; Rajaratnam, R.; Wang, L.; Shi, B. Z.; Kim, B. H.; Yaot, C. F. *J. Am. Chem. Soc.* **1993**, *115*, 10596–10604.

(25) (a) Horowitz, E. D.; Hud, N. *J. Am. Chem. Soc.* **2006**, *128*, 15380–15381. (b) Jain, S. S.; Anet, F. A. L.; Stahle, C. J.; Hud, N. V. *Angew. Chem. Intl. Ed.* **2004**, *43*, 2004–2008.

(26) Wu, W.; Zhong, S.; Shaik, S. *Chem. Phys. Lett.* **1998**, *292*, 7–14.

(27) (a) . Das, K.; Pink, M.; Rajca, S.; Rajca, A. *J. Am. Chem. Soc.* **2006**, *128*, 5334–5335. (b) Rajca, A.; Pink, M.; Mukherjee, S.; Rajca, S.; Das, K. *Tetrahedron* **2007**, *63*, 10731–10742.

(28) Hu, G.; Guo, Y.; Wei, J.; Xie, S. *Phys. Rev. B* **2007**, *75*, 165321/1–165321/6.

(29) (a) Supriyo, B. *J. Nanosci. Nanotechnol.* **2007**, *7*, 168–180. (b) Rocha, A. R.; García-Suárez; V, M.; Bailey, S. W.; Lambert, C. J.; Ferrer, J.; Sanvito, S. *Nat. Mater.* **2005**, *4*, 335–339.

(30) (a) Solomon, E. I. *Inorg. Chem.* **2005**, *44*, 723–726. (b) Dey, A.; Roche, C. L.; Walters, M. A.; Hodgson, K. O.; Hedman, B.; Solomon, E. I. *Inorg. Chem.* **2005**, *44*, 8349–8354.

(31) (a) Hehre, W. J.; Radom, L.; Schleyer, P. v.; Pople, J. *Ab Initio Molecular Orbital Theory*; Wiley-Interscience: New York, 1986. (b) Cramer, C. J. *Essentials of Computational Chemistry: Theories and Models*, 2nd ed.; John Wiley and Sons: New York, 2004.

(32) Bally, T.; Borden, W. T. *Rev. Comput. Chem.* **1999**, *13*, 1–97.

(33) Lunell, S. *Chem. Phys. Lett.* **1972**, *13*, 93–96.

(34) Pauncz, R. *Fund. World Quantum Chem.* **2003**, *1*, 155–181.

(35) Pople, J. A. *Rev. Mod. Phys.* **1999**, *71*, 1267–1274.

(36) Wilson, S. *Handb. Mol. Phys. Quantum Chem. 2003* **2003**, *2*, 314–373.

(37) (a) Schlegel, H. B. *J. Phys. Chem.* **1988**, *92*, 3075–3078. (b) Chen, W.; Schlegel, H. B. *J. Chem. Phys.* **1994**, *101*, 5957–5968.

(38) He, Z.; Kraka, E.; Cremer, D. *Int. J. Quantum Chem.* **1996**, *57*, 157–172.

(39) He, Y.; Cremer, D. *Theo. Chim. Acta* **2000**, *105*, 132–144.

(40) (a) Koch, W.; Holthausen, M. C. *A Chemist's Guide to Density Functional Theory*, 2nd ed.; Wiley-VCH: Weinheim, 2001. (b) Parr, R. G.; Weitao, Y. *Density-Functional Theory of Atoms and Molecules, International Series of Monographs on Chemistry*; Oxford University Press: Oxford, U.K., 1994.

(41) Wittbrodt, J. M.; Schlegel, H. B. *J. Chem. Phys.* **1996**, *105*, 6574–6577.

(42) Noodleman, L.; Lovell, T.; Han, W.-G.; Li, J.; Himo, F. *Chem. Rev.* **2004**, *104*, 459–508.

(43) Fuchs, M.; Niquet, Y.-M.; Gonze, X.; Burke, K. *J. Chem. Phys.* **2005**, *122*, 094116/1–094116/13.

(44) Glendening, E. D.; Badenhoop, J. K.; Weinhold, F. *J. Comput. Chem.* **1998**, *19*, 628–646.

(45) *GaussView, Version 3.09*, Dennington II, R.; Keith, T.; Millam, J.; Eppinnett, K.; Hovell, W. L.; Gilliland, R. Semichem, Inc.: Shawnee Mission, KS, 2003.

(46) Frisch, M. J. ; Trucks, G. W.; Schlegel, H. B.; Scuseria, G. E.; Robb, M. A.; Cheeseman, J. R.; Montgomery, Jr., J. A.; Vreven, T.; Kudin, K. N.; Burant, J. C.; Millam, J. M.; Iyengar, S. S.; Tomasi, J.; Barone, V.; Mennucci, B.; Cossi, M.; Scalmani, G.; Rega, N.; Petersson, G. A.; Nakatsuji, H.; Hada, M.; Ehara, M.; Toyota, K.; Fukuda, R.; Hasegawa, J.; Ishida, M.; Nakajima, T.; Honda, Y.; Kitao, O.; Nakai, H.; Klene, M.; Li, X.; Knox, J. E.; Hratchian, H. P.; Cross, J. B.; Bakken, V.; Adamo, C.; Jaramillo, J.; Gomperts, R.; Stratmann, R. E.; Yazyev, O.; Austin, A. J.; Cammi, R.; Pomelli, C.; Ochterski, J. W.; Ayala, P. Y.; Morokuma, K.; Voth, G. A.; Salvador, P.; Dannenberg, J. J.; Zakrzewski, V. G.; Dapprich, S.; Daniels, A. D.; Strain, M. C.; Farkas, O.; Malick, D. K.; Rabuck, A. D.; Raghavachari, K.; Foresman, J. B.; Ortiz, J. V.; Cui, Q.; Baboul, A. G.; Clifford, S.; Cioslowski, J.; Stefanov, B. B.; Liu, G.; Liashenko, A.; Piskorz, P.; Komaromi, I.; Martin, R. L.; Fox, D. J.; Keith, T.; Al-Laham, M. A.; Peng, C. Y.; Nanayakkara, A.; Challacombe, M.; Gill, P. M. W.; Johnson, B.; Chen, W.; Wong, M. W.; Gonzalez, C.; and Pople, J. A. *Gaussian 03*, revision D.01; Gaussian, Inc.: Wallingford, CT, 2004.

(47) Adam, W.; Harrer, H. M.; Kita, F.; Nau, W. M. *Adv. Photochem.* **1998**, *24*, 205–254.

(48) (a) Konkin, A. L.; Roth, H. K.; Schroedner, M.; Nazmutdinova, G. A.; Aganovb, A. V.; Idac, T.; Garipov, R. R *Chem. Phys.* **2003**, *287*, 377–389. (b) Kawai, A.; Okutsu, T.; Obi, K. *Chem. Phys. Lett.* **1992**, *198*, 637–640.

(49) Adamo, C.; Subra, R.; Di Matteo, A.; Barone, V. *J. Chem. Phys.* **1998**, *109*, 10244–10254.

(50) Adamo, C.; Barone, V.; Subra, R. *Theor. Chem. Acta* **2000**, *104*, 207–209.

(51) (a) Sui, Y.; Glaser, R.; Sarkar, U.; Gates, K. *J. Chem. Theory Comput.* **2007**, *3*, 1091–1099. (b) For 1MA, see: Sui, Y. Ph.D. Dissertation, University of Missouri-Columbia, 2007.

(52) Gerson, F.; Huber, W. *Electron Spin Resonance Spectroscopy for Organic Radicals*, 1st ed.; Wiley-VCH: Weinheim, 2001.

(53) Dust, J. M.; Arnold, D. R. *J. Am. Chem. Soc.* **1983**, *105*, 1221–1227.

(54) Creary, X. *Acc. Chem. Res.* **2006**, *39*, 761–771.

(55) Wen, Z.; Li, Z.; Shang, Z.; Cheng, J. P. *J. Org. Chem.* **2001**, *66*, 1466–1472.

(56) Adam, W.; Kita, F.; Harrer, H. M.; Nau, W. M.; Zipf, R. *J. Org. Chem.* **1996**, *61*, 7056–7065.

(57) Wu, Y. D.; Wong, C. L.; Chan, K. W.; Ji, G. Z.; Jiang, X. K. *J. Org. Chem.* **1996**, *61*, 746–750.

(58) Hippler, H.; Troe, J. *J. Phys. Chem.* **1990**, *94*, 3803–6.

(59) Ellison, G. B.; Davico, G. E.; Bierbaum, V. M.; DePuy, C. H. *Int. J. Mass Spectrom. Ion Processes* **1996**, *156*, 109–131.

(60) Ervin, K. M.; DeTuri, V. F. *J. Phys. Chem. A* **2002**, *106*, 9947–9956.

(61) Finkelshtein, E. I. *J. Phys. Org. Chem.* **2001**, *14*, 543–550.

(62) Kromkin, E. A.; Tumanov, V. E.; Denisov, E. T. *Neftekhimiya* **2002**, *42*, 3–13.

(63) Bauschlicher, C. W.; Langhoff, S. R. *Mol. Phys.* **1999**, *96*, 471–476.

(64) Shurki, A.; Hiberty, P. C.; Dijkstra, F.; Shaik, S. *J. Phys. Org. Chem.* **2003**, *16*, 731–745.

(65) Roberts, J. S.; Szwarc, M. *J. Chem. Phys.* **1948**, *16*, 981–3.

(66) (a) Morato, M.; Caceres, J. O.; Gonzalez Urena, A *Eur. Phys. J. D* **2006**, *39*, 199–208. (b) Rudolph, H. D.; Dreizler, H.; Jaeschke, A.; Wendling, P. *Z. Naturforsch. A* **1967**, *22*, 940–944.

(67) Kruglyak, Y. A.; Ukrainskii, I. I.; Preuss, H.; Janoschek, R. *Teoreticheskaya i Eksperimental'naya Khimiya* **1971**, *7*, 815–819. (AN 1972:92226)

(68) Ohno, K.; Kimura, J.; Yamakita, Y. *Chem. Phys. Lett.* **2001**, *342*, 207–219.
(69) Middleton, B. A.; Partington, J. R. *Nature* **1938**, *141*, 516–517.
(70) Smit, W. M. A.; Van Dam, T. *J. Chem. Phys.* **1980**, *72*, 3658–3662.
(71) Bulgarevich, S. B.; Bren, D. V.; Movshovich, D. Ya.; Filippov, S. E.; Olekhnovich, E. P.; Korobka, I. V. *Russ. J. Gen. Chem.* **2002**, *72*, 1446–1452.
(72) Ewig, C. S.; Waldman, M.; Maple, J. R. *J. Phys. Chem. A* **2002**, *106*, 326–334.
(73) Doerksen, R. J.; Thakkar, A. J. *J. Phys. Chem. A* **1999**, *103*, 10009–10014.
(74) Perez-Casas, S.; Hernandez-Trujillo, J.; Costas, M. *J. Phys. Chem. B* **2003**, *107*, 4167–4174.
(75) Khajehpour, M.; Kauffman, J. F *J. Phys. Chem. A* **2000**, *104*, 9512–9517.
(76) Glaser, R.; Lewis, M.; Wu, Z. *J. Phys. Chem. A* **2002**, *106*, 7950–7957.
(77) Glaser, R.; Choy, G. S.-C. *J. Phys. Chem.* **1993**, *97*, 3188–3198.
(78) Glaser, R.; Choy, G. S.-C. *J. Phys. Chem.* **1994**, *98*, 11379–11393.
(79) (a) Glaser, R.; Chen, G. S.; Grützmacher, H. *J. Comput. Chem.* **1997**, *18*, 1023–1035. (b) Glaser, R.; Choy, G. S. C.; Chen, G. S.; Grützmacher, H. *J. Am. Chem. Soc*. **1996**, *118*, 11617–11628.
(80) Worsnop, S. K.; Boyd, R. J.; Sarasola, C.; Ugalde, J. M. *J. Chem. Phys.* **1998**, *108*, 2824–2830.

JP8011987